Testing the Paradigm that Ultra-Luminous X-ray Sources as a Class Represent Accreting Intermediate-Mass Black Holes

C. T. Berghea

Department of Physics, The Catholic University of America, Washington, DC 20064

79berghea@cua.edu

K. A. Weaver

Laboratory for High Energy Astrophysics, NASA's Goddard Space Flight Center, Greenbelt, MD 20771

kweaver@milkyway.gsfc.nasa.gov

E. J. M. Colbert

Department of Physics and Astronomy, Johns Hopkins University, Baltimore, MD 21218

colbert@jhu.edu

and

T. P. Roberts

Department of Physics, Durham University, South Road, Durham DH1 3LE, UK

t.p.roberts@durham.ac.uk

ABSTRACT

To test the idea that ultraluminous X-ray sources (ULXs) in external galaxies represent a class of accreting Intermediate-Mass Black Holes (IMBHs), we have undertaken a program to identify ULXs and a lower luminosity X-ray comparison sample with the highest quality data in the *Chandra* archive. We establish a general property of ULXs that the most X-ray luminous objects possess the flattest X-ray spectra (in the *Chandra* band pass). No prior sample studies have established the general hardening of ULX spectra with luminosity. This hardening occurs at the highest luminosities (absorbed luminosity $\geq 5 \times 10^{39}$ erg s^{-1}) and is in line with recent models arguing that ULXs are actually stellar-mass black holes. From spectral modeling, we show that the evidence originally taken

to mean that ULXs are IMBHs - i.e., the "simple IMBH model" - is nowhere near as compelling when a large sample of ULXs is looked at properly. During the last couple of years, *XMM-Newton* spectroscopy of ULXs has to some large extent begun to negate the simple IMBH model based on fewer objects. We confirm and expand these results, which validates the *XMM-Newton* work in a broader sense with independent X-ray data. We find (1) that cool disk components are present with roughly equal probability and total flux fraction for any given ULX, regardless of luminosity, and (2) that cool disk components extend below the standard ULX luminosity cutoff of 10^{39} erg s^{-1}, down to our sample limit of $10^{38.3}$ erg s^{-1}. The fact that cool disk components are not correlated with luminosity damages the argument that cool disks indicate IMBHs in ULXs, for which a strong statistical support was never made.

Subject headings: galaxies: general — surveys — X-rays:binaries — accretion, accretion discs

1.   INTRODUCTION

Ultraluminous X-ray Sources (ULXs) have long been hailed as direct observational evidence for the existence of accreting Intermediate-Mass Black Holes (Colbert & Mushotzky 1999). The X-ray spectral model that has emerged as a central pillar for this argument (the "simple IMBH model") is that which is commonly applied as the canonical X-ray spectral fit to Galactic black-hole binaries with stellar-mass black holes (McClintock & Remillard 2006). This model consists of a thermal accretion disk component plus a power-law continuum component. When applied to ULX spectra, the derived disk temperatures are $0.1-0.3$ keV (e.g. Miller, Fabian & Miller 2004), much lower than Galactic black holes (at $0.6-1$ keV). A cooler disk implies a bigger disk - so assuming the disk approximately extends inward to the last stable orbit around the black hole, this would imply bigger, and more massive, black holes. Such cool disks were indeed found in a few ULXs (e.g. Miller, Fabian & Miller 2004).

To counter this argument, many recent papers have pointed out both theoretical and observational problems with the simple IMBH model as a global explanation for all ULXs (e.g. Gonçalves & Soria 2006; Stobbart, Roberts & Wilms 2006; Roberts 2007). The observed accretion disk components can be fairly weak and thus do not provide a reliable measure of black hole mass. Also, the simple IMBH model does not necessarily approximate well the X-ray spectra of many ULXs. Attention has switched to perhaps less exotic models to explain some of the ULXs, such as beaming (King et al. 2001) or super-Eddington accretion (Begelman 2002), both of which explain ULX X-ray properties without the need for an

IMBH. Galactic super-Eddington sources are known, such as stellar-mass black hole binaries like GRS 1915+105 (Fender & Belloni 2004), V4641 Sgr (Revnivtsev et al. 2002) and possibly SS 433. The latter could be an example of both beaming *and* super-Eddington emission, the combination of which could easily explain even the most luminous ULXs (Begelman, King & Pringle 2006; Poutanen et al. 2007). Cool accretion disks can also be physically explained by "coupled disk-corona" models Done & Kubota (2006), blurred emission and absorption lines from surrounding (outflowing) gas (Gonçalves & Soria 2006), or a microblazar with magnetized jets (Freeland et al. 2006), that can transfer disk energy into the jet (thus making the disk fainter and cooling the disk at the same time).

Recent detailed X-ray spectral modeling has revealed properties that complicate further any simple global interpretation, suggesting that multiple classes of ULXs exist. Some very bright ULXs have been found by several authors (Zezas et al. 2002; Soria et al. 2007; Soria & Wong 2006) to have relatively flat spectra, not usually expected in high states for accretion states of black holes (McClintock & Remillard 2006). A flat spectrum suggests an inverse correlation between the slope of the spectrum and source luminosity (see also NGC 5204 X-1, Roberts et al. 2006). Such an inverse correlation is hard to explain with current IMBH models because in the typical high state the spectrum is soft, dominated by the disk component and with a steep power-law (McClintock & Remillard 2006). Specifically, XMM spectroscopy of ULXs has to some large extent already begun to directly negate the simple IMBH model (see for instance Stobbart, Roberts & Wilms 2006; Gonçalves & Soria 2006).

Two *Chandra* surveys suggest that ULXs may in fact be an extension of normal lower-luminosity galaxy populations to higher luminosities. Using simple power-law models applied to spectra with typically 50 counts each, Swartz et al. (2004) compared ULXs to a lower luminosity sample of X-ray sources with $L_X = 10^{38}-10^{39}$ erg s^{-1} and found both distributions of photon indices to be well fitted by Gaussians centered at about 1.9. The samples also have similar X-ray colors, time series and positions within their host galaxies. In another *Chandra* study, Colbert et al. (2004) found no discernible difference between the X-ray colors of ULXs and lower luminosity sources in spiral galaxies. Both analyzes were done with data of fairly poor spectral quality in terms of fitting detailed models and the latter relied on a color-color analysis rather than spectral fitting, per se. These works also did not include two-component model fits that would identify spectral states and directly test the simple IMBH model

To search carefully for spectral properties that can differentiate ULXs, we need the best data available that will allow us to distinguish between simple spectral models. In this paper we use the highest quality X-ray spectra for a large, complete sample of ULXs from the Chandra archives to test various ULX models. We are able to provide a statistically strong

comparison of the results with lower-luminosity X-ray sources of equal data quality. We pay special attention to properties usually associated with ULXs, such as the signature of a cool disk, which has never been tested for a uniform and large sample of good quality *Chandra* spectra. Is the cool disk preferentially found in ULXs? If yes, does the disk dominate the total emission? We also search for other spectral behaviors found more recently in individual ULXs, such as a correlation between hardness and luminosity, and what this might mean. For the first time, strong statistical tests of various ideas of ULX models can be provided to the ULX community.

With its unmatched spatial resolution, *Chandra* is better suited than *XMM-Newton* for studying point sources in crowded regions or resolving point sources in distant galaxies. This is particularly true for the starburst galaxies that host populations of ULXs (e.g NGC 3256, Lira et al. 2002; Cartwheel galaxy, Gao et al. 2003), where only *Chandra*'s unparalleled X-ray optics can spatially and spectrally resolve the emission from ULXs from that of the underlying galaxy. We have searched all public data available in the *Chandra* archive for ULXs and lower-luminosity comparison objects with at least 1000 counts. In section 2 we present our source selection process, methods for identifying rejected objects, and an estimate of contamination from background objects. In section 3 we discuss the spectral fitting procedures and compare the spectral properties of the two samples. Our goal is to determine whether ULXs as a class have different spectral properties than the less luminous, "normal" X-ray sources and to offer an improved diagnosis by using the high quality spectral data available in the *Chandra* archive. In section 4 we present results from the variability analysis. Finally, in Section 5 we interpret our results and discuss the insight provided into the nature of ULXs.

2. SAMPLE SELECTION AND OBSERVATIONS

2.1. Sample Criteria

There are many published papers that address the nature of ULXs. These analyses are typically drawn from heterogeneously selected samples, small numbers of objects, or large samples with limited data quality (Swartz et al. 2004; Colbert et al. 2004). Comparisons of ULXs with other types of X-ray point sources in nearby galaxies often use selection criteria that do not provide the spectral data quality that allows a robust set of statistical conclusions to be drawn from data modeling. In this work, we use criteria that create the best possible available sample to address the nature of ULXs by defining a large and statistically robust sample of ULXs and other point-like X-ray sources in nearby galaxies with uniform data quality. Uniformity of data quality is our prime objective and the completeness of our

sample is limited by the observations that are available in the *Chandra* archive - most of which have been obtained by other researchers for a variety of purposes.

Our ULX and comparison samples are statistically robust in the sense that we include all point sources in *Chandra* archive with at least 1000 counts and a luminosity above $10^{38.3}$ erg s^{-1}. We carefully reject sources associated with active galactic nuclei, supernovae and foreground stars. We also reject piled-up observations to simplify our spectral analysis. *Chandra* provides the most accurate X-ray positions to date and thus we can be sure to identify well-isolated objects for our study. Several *XMM-Newton* studies of ULXs are published, but while these individual spectra are of higher quality, there are fewer individual point sources available due to *XMM's* poorer imaging resolution and source confusion for faint targets located in crowded regions in galaxies. We have not made our sample fully representative in the sense of picking the same number of ULXs and comparison objects from similar galaxy types. Conclusions about the distribution of objects according to galaxy type can, however, be inferred from our statistical comparisons. Uniformly good-quality X-ray spectra allow us to apply exactly the same physical models to the ULX and comparison samples and directly compare results within the sensitivity limits.

There are selection biases inherent in our analysis. One is distance. For sources that are intrinsically less luminous, a larger fraction of objects will be located in the nearest host galaxies, while more luminous objects can be utilized from galaxies at greater distances. We also do not select objects according to any specific requirement on their local environments (their locations in their host galaxies, for example).

2.2. Initial Sample

Our sample is derived from the list of X-ray point sources generated by the XASSIST[1] *Chandra* pipeline. For manageability, we have chosen all *Chandra* ACIS sources in the public archives as of a cutoff date of October 18, 2004. We determine which XASSIST sources are associated with host galaxies following the procedure used by Colbert & Ptak (2002). X-ray sources are further considered if they are located inside the D_{25} ellipse of their host galaxy. Parameters for the D_{25} ellipse are obtained from v3.9b of the Third Reference Catalog of Bright Galaxies (RC3; de Vaucouleurs et al. 1991). We further only consider RC3 galaxies with recessional velocities $cz \leq 5000$ km s^{-1}.

---

[1]XASSIST (Ptak & Griffiths 2003) is a semi-automatic X-ray analysis program written and maintained by A. Ptak. Analysis of archival data processed by XASSIST can be found at the URL www.xassist.org.

To estimate observed X-ray luminosities L_{XA}, we calculated the $0.3-8.0$ keV fluxes with XASSIST assuming a power-law model with $\Gamma = 1.8$ and Galactic absorption and used distances for the associated RC3 galaxies. For galaxies with $cz < 1000$ km s^{-1}, distances were taken from Tully (1988), otherwise distances were computed using $H_0 = 75$ km s^{-1} Mpc^{-1}. We retained all sources with $L_{XA} > 10^{38.3}$ erg s^{-1} and then manually inspected the X-ray images to eliminate false X-ray sources chosen by the automatic data processing. This initial selection yielded 126 unique X-ray point sources in 188 *Chandra* observations. A significant fraction of the point sources were observed multiple times, which provides some useful variability information.

2.3. Obvious Rejected objects (AGNs, QSOs, SNe, Stars & Jets)

To reject X-ray point sources unrelated to our science, we used the NED[2] database. The absolute positional uncertainty for *Chandra* ACIS images is better than $1''$ (e.g. Weisskopf et al. 2003), which provides the accuracy requirement needed to identify an optical, infrared or radio counterpart. Optical positions provided by NED are typically accurate to within a few arc seconds and positions may be slightly less accurate for infrared and radio sources, so we first searched NED using a radius of $5''$ surrounding the XASSIST position. We next visually inspected the X-ray sources and their possible NED counterparts by overlaying the XASSIST position, the NED position, and the D_{25} galaxy ellipse onto the raw X-ray images and DSS2[3] red images.

Optical images were used to check for bright, foreground star counterparts. We then refined our ID search by examining the literature for more accurate positions for identified NED counterparts. In some cases VLBI measurements are available with sub-milliarcseconds positional accuracy, such as those used by Ma et al. (1998) for the International Celestial Reference Frame (ICRF). Some published 2MASS positions also use the ICRF reference system and have accuracies better than $0.1''$, varying slightly with the source brightness (see UCAC2 catalog, Zacharias et al. 2004). Optical positions that can be correlated with radio measurements show systematic differences of only $0.1''$ (e.g. Argyle & Eldridge 1990). Overall, we determined that the positional uncertainties of identified counterparts are generally much smaller than our X-ray positional uncertainties, the largest uncertainty being $1''$. We

---

[2]NASA/IPAC Extragalactic Database, URL NEDWWW.IPAC.CALTECH.EDU

[3]The Second Digitized Sky Survey consists of high resolution scans of several plate collections in the red, blue, visible and near infrared. The images were downloaded from the server installed at ESO, using a remote client, ESO/ST-ECF Digitized Sky Survey application.

estimate a conservative upper limit of 1.5″ for the net uncertainty in separation between the *Chandra* X-ray source and an identified optical, IR or radio counterpart for any object in our sample. Therefore, we feel confident that we have identified correct counterparts to within the errors provided by the X-ray data.

From this search we reject 32 X-ray sources out of 69 *Chandra* observations. Most are associated with Seyfert and Liner galaxies (Ho, Filippenko & Sargent 1997; Véron-Cetty & Véron 2003; Bryant & Hunstead 1999). Others include background quasars and point-like X-ray knots associated with jets within the host galaxy. As an example, source 37 in Zezas et al. (2002) in the Antennae galaxy pair (NGC 4038/9), is a background quasar with redshift 0.26 (Clark et al. 2005). We identified a supernova in NGC 891 (SN 1986J; Bietenholz, Bartel & Rupen 2002). One ULX in M101 (NGC 5457 X-6 in Roberts & Warwick 2000) is actually a foreground star, GSC2.2 3842. After rejecting sources based on optical and NED counterparts we are left with 94 X-ray sources in 119 *Chandra* observations.

2.4. Reprocessing of Archival Data and Final Rejection Criteria

Having narrowed our sample according to the above criteria, the ACIS imaging data were retrieved from the *Chandra* archives. The level-1 event files were reprocessed with CIAO v3.0.1 and CALDB v1.4, using the ACIS_PROCESS_EVENTS tool. No adjustment was made for charge transfer inefficiency (CTI) effects between pixels during the data readout. This allows the analysis of data to be uniform for different CCD detectors and degrees of CCD pile-up. To minimize pile-up effects, we restricted the count rates for on-axis full-frame (frame time 3.24 s) CCD observations to be < 0.08 s^{-1}. According to the *Chandra* Proposer's Observatory Guide (v.4)[4], this corresponds to 10% pile-up. Count rates in excess of this value for point sources are likely to impact the extracted spectra. PHA randomization was applied, but pixel randomization was not.

In cases where the X-ray sources are observed off-axis or in a subarray CCD mode the pile-up effect is reduced and we can accept a higher net count rate. The actual pile-up fraction is estimated for the "reduced" count rates in Table 1. These count rates were calculated by taking into account the larger point-spread function for sources observed off-axis and the CCD observation mode. Column 8 lists the ACIS CCD in which the source is imaged and the subarray value, i.e., the fraction of the CCD used in the observation. Exposing a smaller chip area results in shorter frame times and reduces the pile-up.

---

[4]http://cxc.harvard.edu/proposer/POG/

Source spectra were typically extracted from regions of radius $2''$, and local background spectra were extracted using annuli with inner and outer radii of $6''$ and $10''$. For off-axis sources we used elliptical regions, and for crowded regions, slightly more complicated background regions, as needed. Visual inspection ensured that there is no confusion with any nearby X-ray sources. Sources were retained that had > 1000 counts in the reprocessed data. Spectral fitting was performed using XSPEC v11.2.0bd.

A total of 21 sources had less than 1000 counts after the archival data were fully reprocessed and so these are rejected. In addition, 9 observations of 7 sources have $> 10\%$ pile-up and are rejected (Table 1). Most of the sources with significant pile-up have other *Chandra* observations, and so only 3 unique objects are fully rejected from our sample because of pile-up, 2 ULXs and one lower-luminosity source.

2.5. Final Sample

A total of 69 unique objects in 89 datasets comprise our final sample. The properties of these objects are listed in Table 2, together with some properties of their host galaxies. Using count rates derived from our reprocessed data, we re-computed the $0.3-8.0$ keV observed luminosities (L_X), using a power-law model with $\Gamma = 1.8$ and Galactic absorption. A final division into two groups is made according to the maximum observed luminosity, L_X^{max}. There are 47 ULXs ($L_X^{max} \geq 10^{39.0}$ erg s^{-1}) and 22 comparison objects of lower-luminosity ($L_X^{max} < 10^{39.0}$ erg s^{-1}).

Some sources show luminosity variability. For two ULXs, U2 (M33 X-8) and U41 (IXO 83), their luminosity can fall below our threshold value of $10^{39.0}$ erg s^{-1} in some cases, but we still retain the classification of ULX. Our method identifies a ULX as such if it is observed with $L_X \geq 10^{39.0}$ erg s^{-1} at least once. On the other hand, a well-known and previously studied ULX, IXO 85 (C22) is excluded from our ULX sample because the *Chandra* luminosity falls just below our ULX limit.

Examining the galaxy properties in Table 2, we find that most of our sample objects reside in spiral or irregular (merger) galaxies, and are preferentially located in spiral arms and star forming regions. Our galaxy sample includes two mergers (NGC 520 and The Antennae), and four early type galaxies (NGC 2681, NGC 4125, M87 and Cen A). We see little difference between the ULX locations in their host galaxies in general and the locations of the comparison sources. The two groups also tend to have similar deprojected offsets from the centers of their galaxies. Two ULXs (U2 and U14) are associated with the nucleus of their host galaxies (M33 and NGC 3310, respectively), but with no evidence for AGN activity. We

do not have enough detailed information on these sources to know what fraction are known low-mass X-ray binaries (LMXB) and high-mass X-ray binaries (HMXB). The identification of the optical counterparts would require sensitive optical imaging. Based on the location in the host galaxy we can only say that most of our sources in both samples are consistent with being HMXBs.

2.6. Background Contamination

Here we estimate potential sample contamination from additional background objects that have not already been clearly identified. We use the $\log(N)-\log(S)$ function from X-ray deep field surveys to estimate the fraction of additional background objects based on our source fluxes and galaxy distances. For our sample criteria, we construct two flux limits, FL and FC. FL is the flux of a source with a specific luminosity: $10^{39.0}$ erg s^{-1} for ULXs and $10^{38.3}$ erg s^{-1} for our comparison sample. FC is the flux of a source that provides 1000 counts in its spectrum for the longest exposure time obtained for each galaxy. Assuming a power-law model with $\Gamma = 1.8$ and using the Galactic value of absorption corresponding to the location of the center of each galaxy on the sky we calculate FL and FC for all of the 286 galaxies in our original list (see section 2.1). The final flux limit for each galaxy to compare with $\log(N)-\log(S)$ is the largest of the two fluxes, FC or FL. All of our measured fluxes are above 10^{-14} erg cm^2 s^{-1}, which corresponds to an ACIS count rate of $\sim 10^{-3}$ s^{-1}.

To make a background estimate we also need to account for the size of the detectors on the sky compared to the projected sizes of the galaxies. The area of each galaxy in deg^2 was first calculated within the D$_{25}$ ellipse. Most observations are done in ACIS imaging mode, with detector areas of ~ 0.117 deg^2 for both ACIS-I and ACIS-S. Data can be extracted from specific CCD chips and some observations only occur on subarray mode with a significantly smaller exposed area. The disparity between the sizes of the galaxies and the detector coverage can effect our background estimates. For the nearest galaxies, their size on the sky is larger than or comparable to the size of the ACIS detectors. Naturally, if the projected area of the galaxy is larger than or comparable to the size of the detector, these galaxies will provide the largest estimated contributions to the background counts. We therefore accounted for the fractional coverage of the 13 largest galaxies by over plotting the CCDs and estimating the coverage fraction. These 13 galaxies (out of the original 286) contribute 65% to the total estimate of the contamination. For the remaining galaxies we use the D$_{25}$ ellipse area.

We used the $\log(N)-\log(S)$ function from two separate surveys to obtain flux estimates. The popular *ROSAT* deep survey in the Lockman Hole (Hasinger et al. 1998) gives

log(N)−log(S) for the flux interval 10^{-15}−10^{-13} erg cm^2 s^{-1}, in the range 0.5−2 keV. We applied a scale factor of 0.38 for our 0.3−8 keV band, obtained using the absorbed power-law model with $\Gamma = 1.8$. The *Chandra* Multiwavelength Project (ChaMP) serendipitous survey (Kim et al. 2004), contains a larger sample, and covers a wide area ($\sim$14 deg^2). It uses the same soft X-ray band as the *ROSAT* deep survey but the slope of the log(N)−log(S) function is shallower at the high end.

For ULXs, the ROSAT and ChaMP surveys predict no more than 3 or 5 spurious sources, respectively. For our lower luminosity objects, the prediction is 1 or 2 spurious sources. The survey estimates are compatible given large errors due to poor sampling at the high flux end. Thus no more than approximately one in ten sources in our sample is likely a background object. In a practical sense this is an upper limit, as our estimate does not take into account the variable absorption column through each galaxy, which will attenuate the signal of any background sources shining through the galaxy (i.e. reduce their observed flux). This is especially important as we have used surveys in the 0.5−2 keV band where absorption is strong. We also remind our reader that we had already identified and rejected two background quasars (Section 2.3).

3. SPECTRAL ANALYSIS

We grouped the spectra to have a minimum of 15 counts per energy bin for the energy range of 0.3−8.0 keV. All fits were performed using the Galactic absorbing column (as listed in Table 2), plus an intrinsic absorbing column for each galaxy. Galactic values were obtained with the COLDEN routine in CIAO, which provides a foreground N$_H$ value at a given celestial position. We choose to define acceptable (or "good") fits to be those for which $\chi^2_\nu \leq 1.2$. Unless specified, all errors quoted are 90% confidence for one interesting parameter ($\Delta\chi^2 = 2.7$). For sources with multiple observations, the individual observations were first fitted separately and then all observations were fitted together in XSPEC for the various purposes of our work. Simultaneous fits are used in the histograms and listed in tables (e.g. Table 3) and individual fits are shown in some of the plots to demonstrate any variability in luminosity and spectral shape. For the simultaneous fits, the model parameters were constrained to the same value in XSPEC and only the normalizations of model components were allowed to vary freely.

In a statistical sense, spectral fitting results can be strongly biased by the number of counts in each spectrum. To test for such biases between the ULX and the comparison samples, we constructed histograms of net counts in the spectra (see Figure 1). For sources with multiple observations, we chose the observation that contains the largest number of

counts in its spectrum (see Table 2) to represent in the histogram. The distribution of number of counts for objects in the samples are similar. A Kolmogorov-Smirnov (K-S) test provides a probability of 0.86, indicating that we have no reason to reject the hypothesis that the distributions are the identical in counts space. Thus the two samples have equal sensitivity to spectral features for our model fitting.

3.1. Single-Component Spectral Fits

Recent spectral analysis of Chandra ULX spectra show that many are well fitted by simple models (e.g. Humphrey et al. 2003; Swartz et al. 2004). We therefore fit all spectra with either an absorbed power-law (PL) model or a multi-color disk blackbody (MCD) model, with absorption fixed at the Galactic value in XSPEC. To keep our results within physical bounds, we imposed upper limits of $\Gamma \leq 10$ and $kT_{in} \leq 4$ keV, respectively. Results are listed in Table 3. Both the ULX and comparison samples are generally well fitted by the absorbed PL model (66% and 50%, respectively are good fits, as marked in column 10). For the absorbed MCD model, good fits comprise 45% and 50% of the samples, respectively.

The histograms in Figure 2 show the distributions of photon index and inner disk temperature, normalized to allow for an easy comparison. For the full sample, we find no significant difference between ULXs and lower luminosity objects. Luminosity dependences are presented in Figure 3. For objects that have multiple observations, all fit results are shown.

We have applied the Kolmogorov-Smirnov (K-S) test and the T-test to the samples in different ways. This first row of Table 4 shows the results of the test applied to the total set of fits, while the second row is restricted to the "good" fits as defined in the first paragraph of Section 3. All calculated probabilities are higher than a 5% significance level, confirming that there are no significant differences when comparing the distributions or their means. We note that the derived probabilities differ in some cases significantly between the K-S test and the T-test, which is an indication that the distributions plotted in Figure 2 are possibly derived from intrinsic samples that do not have normal distributions and/or that our sample sizes are small (such tests are usually more reliable when applied to large samples).

Even with these caveats, we find an interesting trend if we limit our sample further. When only considering the good fits, the disk temperatures are marginally higher for ULXs (at 1.8 keV, with a significance level of 7-8%). If we further use Figure 3a to split the ULXs themselves into two groups, with a luminosity break at 5×10^{39} erg s^{-1}, then we find that the highest luminosity ULXs have significantly harder X-ray spectra than both the lower

luminosity ULXs or the comparison sample (rows 3-6 of Table 4).

Our primary result from applying single-component models is that all of the highest luminosity ULXs that are well fitted by the PL model possess hard X-ray spectra ($\Gamma \leq 2$ and $kT_{in} \geq 1.3$ keV). The most luminous ULXs have harder spectra and those less luminous have spectral shapes similar to the comparison sample. Not all of the high-luminosity ULXs have hard spectra, however, and so we have further defined a subsample of 9 very luminous and hard ULXs (inside the upper left corner rectangle in Figure 3a): U4, U5, U10, U11, U14, U18, U19 (with 4 observations), U20 and U43. These all have luminosities in excess of 5×10^{39} erg s^{-1} and photon indices < 1.7. This subclass will be discussed further in the next sections.

3.2. Two-Component Spectral Fits

We next fit all spectra with the frequently used the two-component model that consists of a disk blackbody model (MCD) plus a power-law. Typical spectral states observed in black hole binaries and some ULXs (e.g. Kubota et al. 2001) include a soft (high) state, with a prominent blackbody component having kT ~ 1 keV plus a steep ($\Gamma \sim 2.5$) power-law tail, or a hard (low) state with the thermal component being generally cooler or nonexistent and most of the energy carried in a shallower power-law ($\Gamma \sim 1.8$). We also mention the Very High State (VHS) characterized by high luminosities, a steep power-law ($\Gamma > 2.5$), a relatively cool disk, and sometimes X-ray quasi-periodic oscillations (QPOs, see McClintock & Remillard 2006, for a detailed description).

We note that these spectral states have been traditionally measured in the $2-20$ keV energy band and therefore may not be recognized easily in the *Chandra* band. For example, in the high state the power-law component would be completely absent in our $0.3-8$ kV band. Also, one of the most important signatures expected from an IMBH is a cool accretion disk component. The inner disk temperature in the MCD model scales with the black hole mass as $\propto M^{-1/4}$. For typical values of $kT_{in} \sim 1$ keV for a black hole binary with a $10M_{\odot}$ in high state, we would expect cool disks with $kT_{in} \sim 0.1-0.3$ keV. A number of ULXs with high quality spectra from *Chandra, XMM-Newton,* and *RXTE* were found in the past few years to show soft components well fit by an MCD model in this range (see Miller, Fabian & Miller 2004).

To compare with published results and restrict model parameters enough to be useful for our purposes, we selected a two component model with fixed parameters. We assume inner disk temperatures of 0.25 or 1 keV, to represent either a cool disk or a "normal" disk

temperature, respectively (models PLMCD0.25 and PLMCD1.0). For ULXs, good fits are derived for 70% and 72% of the sample for PLMCD0.25 and PLMCD1.0, respectively. For the comparison sample, good fits are derived for 59% and 55% for PLMCD0.25 and PLMCD1.0, respectively. The ULXs do posses a higher percentage of good fits, but the difference is not statistically significant given our sample sizes. Figure 4 shows the distribution of photon indices. The shaded areas correspond to the subsample of 9 ULXs with high luminosities and hard X-ray spectra as defined in the previous section (see Figure 3a). In total, there is no significant difference between the ULXs and the lower-luminosity sources. A K-S test for the difference between the distributions gives probabilities of 0.21 and 0.15 for PLMCD0.25 and PLMCD1.0, respectively. However, the 9 high-luminosity, hard ULXs clearly stand out. We note the very steep power-law component in some spectra for the PLMCD1.0 model. These results correspond to the "non-standard model" fits of Stobbart, Roberts & Wilms (2006).

We tried our two-component model with all parameters free (PLMCD model) but many parameters are not constrained. Moreover, as seen in Figure 5, the MCD component is very weak or practically non-existent in many cases. The nine high-luminosity, hard ULXs have the weakest disk components, practically negligible. We note a very steep power-law component in some spectra here, again indicating a non-standard model. In these spectra the non-thermal component is soft and strongly absorbed, as shown by the large values of the flux ratios. Here we only comment further on specific results for spectra that were not well fitted with the simple models from Section 3.1. Table 5 presents the PLMCD model results and in Figure 6 we plot absorbed luminosities versus the photon index and disk temperature. The two samples do not show significant differences. Both samples possess cool disks, and there is no apparent correlation of the disk temperature with luminosity. The presence of this soft disk component also causes the power-law slopes to generally become steeper, compared to our single power-law fits (Figure 3).

The use of applying the F-test for an *added* spectral component (Protassov et al. 2002) is controversial and so we performed simulations to check validity of the F-tests. For each spectrum we performed 500 simulations under a null model, a power law (PL) in this case. We first used the command "tclout simpars" available in XSPEC v.12 to generate simulated parameters from the original fits. This method uses simulations from a multivariate normal distribution based on the covariance matrix estimated in the original fit. The simulated F-test results are listed in parentheses in column 7 of Table 5. Any differences between the simulations and the classical F-test are small and generally fall within the errors corresponding to the number of simulations ($\sim 5\%$). The method described in Protassov et al. (2002) uses a complete Bayesian Monte-Carlo simulation to sample from the posterior distribution (developed by van Dyk et al. 2001). Our method *approximates* the posterior distribution

with a multivariate normal distribution centered at the best fit value. This is nevertheless better than just using the "fakeit" command on the original spectrum fitted with the null model (described by Protassov et al. 2002, as a "parametric bootstrap", and only valid when the parameters are very well constrained).

In conclusion, for the subsample of 9 high-luminosity, hard ULXs (Figure 3a and Section 3.1) we recover the same result here - they tend to have significantly harder spectra. We also verify that they tend to possess small contributions from a thermal component. If such a component exists, it is practically undetectable with the *Chandra* data. We also find that cool disks (MCD with $kT_{in} \sim 0.1-0.3$ keV) are present with roughly equal probability for any given ULX and that cool disks componensts extend below the standard ULX luminosity cutoff (10^{39} erg s^{-1}), down to our sample limit of $10^{38.3}$ erg s^{-1}.

4. SHORT-TERM VARIABILITY

Long term flux variability from one observation to another, which is typically years, is very common in ULXs. Short-term flux variability, which we define here as that which can be detected within a single observation (hours) is less frequent, and is not easily found with *Chandra*, probably due to limited sensitivity (i.e., not providing enough counts). Using the K-S test, Swartz et al. (2004) find that $\approx 15\%$ of our ULXs are variable at the 95% confidence level.

We extracted light curves for all sources, using three time bins: 3.24 s (nominal frame time), 500 s and 1000 s. To test for variability, we used the K-S statistic for the nominal frame time binning, and the Chi-Squared test for the other two. Using the Monte Carlo method of Park et al. (2006) described in the previous section, we constructed light curves for the hardness ratios for each variable source and looked for variations in hardness ratios and possible time lags between the three energy bands. We also constructed power spectra using the Leahy normalization.

We detect variability at 95% confidence in 6 ULXs for the longer time frames using the Chi-Squared test, and no variability for the lower luminosity sample. Of these, three sources were previously known to be variable. These are (M33 X-8), U34 and U40. Three other sources show variability. These are U14, U27 and C22, and the variability scale is similar to the the exposure times of the observations ($\sim$40 ks). The K-S test identifies the same variable sources with the exception of U33 in NGC 5055, but it finds significant variability in two additional sources: U27 in NGC 4565 and a comparison source, C22 in NGC 6946. There are two periodicities of 707 s detected in U33 and U6 (NGC 1313 X-1) produced by

the ACIS dither, which causes false periodic signals at 707 s and 1000 s.

We conclude that 6 ULXs are intrinsically variable, which is consistent with the result obtained by Swartz et al. (2004) given the small size of the sample (47 sources). Only two sources (U2 and U40) show some energy variation, but no lag. Given the readout time of the *Chandra* CCDs, variations on timescales shorter than ≈10 s cannot be detected, and features that could identify spectral states (QPOs or breaks in the power density spectra), are not readily detectable.

5. DISCUSSION

From our X-ray spectral comparison between Ultraluminous X-ray Sources (ULXs) and other X-ray point sources in nearby galaxies, we find an interesting subclass of nine ULXs that have unique properties compared to the other sources that are classified as ULXs. This subclass of ULXs also differs from the lower-luminosity sample of X-ray point sources. While most of the ULXs we analyzed can plausibly be explained as scaled-up versions of Galactic black hole binaries, this particular subclass cannot. We discuss this subclass of ULXs followed by our general results, and especially how our results relate to current evidence that supports the idea that ULXs host Intermediate-Mass Black Holes (IMBHs).

5.1. Luminous, Hard (flat-spectrum) X-ray ULXs

Our analysis has identified nine ULXs with very high luminosities and hard (flat) X-ray spectra. This sample (U4, U5, U10, U11, U14, U18, U19, U20 and U43) is shown in the upper left corner rectangle in Figure 3a. These ULXs are all well fitted by a power-law model with a photon index of < 1.7. More complex spectral fitting using two component models reveals that when trying to add an accretion disk component (the MCD model described in the text), the contribution of this component to the total X-ray flux is very small indicating that the relative contribution of emission from the accretion disk to the total spectrum is small. This result is shown in Figure 5, where the ratio of the absorbed MCD component flux to the total flux is plotted against the power-law index for the PLMCD model. By using absorbed fluxes we do not specifically show the absolute physical strength of the accretion disk component, however, the ratios measured in this way better indicate the significance of detecting a soft excess, and are also less dependent on the modeling.

The subclass of nine flat-spectrum ULXs are also very luminous and so they would seem to be the best candidates for hosting an intermediate-mass black hole (IMBH) based

on a simple Eddington limit argument which predicates that higher mass black holes are required to explain the most luminous accreting sources. The spectra of these ULXs resemble Galactic black holes in a hard state, but such spectral shapes are usually associated with a low luminosity state in the case of Galactic black holes. If these ULXs are indeed accreting IMBHs in a low state (i.e. low/hard state), our result begs the question as to why we don't also see ULXs in a high state (high/soft state) with even higher luminosities. Moreover, if these are IMBHs in a low state, such a scenario implies very high mass black holes ($>10^4$ M$_\odot$). The formation of such black holes is not easy to explain.

It seems more plausible that this subclass of hard (flat) and luminous ULXs are accreting sources in the power-law dominated very high state (McClintock & Remillard 2006), with an unusually weak soft X-ray component. A model that describes the properties of a hard power-law with very little flux from disk, at least in the *Chandra* band, is the "coupled disk-corona" model proposed by Done & Kubota (2006). In this model, the underlying accretion disk emission is distorted by a process that drains energy from the disk into the corona. In an extreme case, the inner disk emission could be almost completely comptonized, and thus only the visible outer disk would contribute to the accretion disk component. As this obviously only appears at low temperatures it could be easily absorbed in some galaxies and also hard to detect. However, if our nine luminous ULXs are interpreted as stellar-mass black hole systems in a high state, we would need to explain why their X-ray spectra are much harder compared to those observed in our Galaxy (McClintock & Remillard 2006), which have typical photon indices of 2.5 in the very high state. We would also need to explain how such low-mass black hole systems could reach such high luminosities.

There is some direct evidence that high-luminosity states in ULXs correlate with the hardness of the power-law tail in their spectra. Roberts et al. (2006) have shown this for a long *Chandra* observing campaign of NGC 5204 X-1 (our U36). These data were not available when we searched the archive. Roberts et al. (2006) found that the spectrum becomes harder as the flux increases, over time-scales of days to weeks. The model used was a Comptonized disk model, and the results showed a cool disk ($\sim$0.1 keV) and an optically thick corona. This model demonstrates that flux variations correlate with the corona temperature. Roberts et al. (2006) favor a stellar mass black hole interpretation for this ULX, and suggest an unusual, very high state, probably produced by extreme mass transfer from a massive star. We should note however that the power-law slope is much steeper for NGC 5204 X-1 compared to the ULXs we discuss, therefore much easier to interpret as a very high state in comparison to what is observed for Galactic black holes.

It is possible that our nine ULX spectra appear to be harder than they actually are due to the limited energy band covered by *Chandra*. If these objects intrinsically possess a break

or curvature in their spectra and the break occurs at an energy above the *Chandra* band pass or where the sensitivity of *Chandra* falls off significantly, this might bias our modeling to measuring these sources as "hard". This appears to be the case for one ULX in our sample, NGC 1313 X-1 (U5), Using *XMM-Newton* spectra, Stobbart, Roberts & Warwick (2006) found evidence for a break (or curvature) at 4.9 keV, with a photon index for the high energy power law being 2.16. (much closer to Galactic BH). The authors show, however, that such breaks are easier to explain if ULXs contain stellar-mass BHs rather than IMBHs. The curvature would be likely to originate in optically thick coronae. This theory would need to be tested for the remaining ULXs in our subclass by obtaining better quality spectra.

In conclusion, the subclass of nine ULXs with very high luminosities and hard (flat) X-ray spectra suggest a power-law dominated very high state, in line with recent models of stellar-mass black hole systems in very high accretion states. The fact that the highest luminosity ULXs are explained easier with such models argues strongly against IMBHs as the only explanation of ULXs.

5.2. Cool disks and the IMBH interpretation

Using our sample of ULXs and lower-luminosity X-ray sources we have found that the spectral signature of a cool accretion disc is not specific to ULXs. The results of the widely used PLMCD model (see Figure 6 and Table 5) show that many sources in both samples have MCD components with low inner disc temperatures. Cool disks have been used until recently as support for the IMBH interpretation. Our results show that this evidence is nowhere near as compelling when a large sample of ULXs is looked at properly.

In the standard accretion disk model, cool disks are not expected for stellar-mass black holes accreting near their Eddington limits. The disk temperature scales with the black hole mass as $T_{in} \propto M^{-1/4}$, and for stellar-mass black holes are ~ 1 keV. However, cool disks can be seen in a low (hard) state, because the temperature dependence on the accretion rate for standard disks is $T_{in} \propto \dot{M}^{-1/4}$ (McClintock & Remillard 2006; Miller et al. 2006). Cool disks have indeed been found in some non-ULX sources. (e.g. Stobbart, Roberts & Warwick 2006). The authors note the similarity of these spectral fits with those typically used for ULXs. They also suggest that the soft excess in some cases could be otherwise explained by contamination from the host galaxy.

Most sources in Figure 6b possess low disk temperatures, both within the ULX and comparison samples. Indeed, it is surprising that we don't see many states that are typical (high) states for stellar-mass black hole binaries, with a prominent ~ 1 keV blackbody

component (though a hard power-law tail would be difficult to discern in the limited *Chandra* band pass). Only U2, U37, C3 and C9 show such high temperatures. We find a similar result from our cool disk model (PLMCD0.25). A large fraction of our ULX spectra (70%) are well fitted by this model, but also a significant number of lower-luminosity objects (59%).

There are theoretical models that do not require the presence of an IMBH to explain a cool disk at high accretion rates and high luminosities (i.e., for ULXs). We already mentioned the model proposed by Done & Kubota (2006), that explains cool disks by a process of draining energy from the disk to launch an optically-thick corona that obscures the hot inner regions of the disk. Freeland et al. (2006) developed microblazar models with magnetized jets that cause a transference of disk energy into the jet, thus making the disk fainter and cooling the disk at the same time. Other phenomenological models include the "dual thermal" model of Stobbart, Roberts & Wilms (2006), in which the soft excess comes from an optically-thick outflow produced at high accretion rates (see King & Pounds 2003), which is seen in addition to a disk component with a temperature similar to those seen in stellar-mass black hole binaries. This latter model was proposed to explain the alternate model of Stobbart, Roberts & Wilms (2006).

Done & Kubota (2006) found evidence of a Galactic BH that supports the interpretation of ULXs as stellar-mass BHs in a very high state. The microquasar XTE J1550-564 has a "strong very high state" (cf. also Kubota & Done 2004) where the disc temperature decreases with luminosity, reaching values of $0.3-0.4$ keV. This suggests a new type of a very high state, a so-called "ultraluminous branch", being very similar to ULX spectra (Roberts 2007; Soria et al. 2007). In this interpretation, ULXs represent the high end of such an accretion state, with BH masses up to 100 $M_\odot$ and accretion rates up to 20 times the Eddington limit. Forming black holes with such masses is much easier to explain than forming IMBHs. For example Belczynski, Sadowski & Rasio (2004) showed that black holes with masses of 80 $M_\odot$ or more can form through binary mergers. Soria & Wong (2006) suggested that black holes of up to 200 $M_\odot$ could form by large scale dynamical collapse of protoclusters in active regions in galaxies. These formation mechanisms are supported by the association between ULXs, star forming regions and colliding galaxies.

5.3. Conclusion

We have found that the highest luminosity ULXs tend to have the hardest X-ray spectra in the *Chandra* band pass and are well fitted by a simple power-law model, without evidence for thermal accretion disc components. Such spectra are not consistent with current IMBH models, but are more in line with current models of extreme very high states, or perhaps a

new "ultraluminous state" (Roberts 2007), in stellar-mass BHs.

Our work shows that cool accretion disks are not exclusive to the ULX class, suggesting that low-temperature intermediate-mass black holes are not the only explanation for this phenomena. In general, our results show that ULXs are likely to be composed of several distinct types of objects, and that these types may extend into lower X-ray luminosity classes, such as classical Galactic Black Hole Candidates, and other objects in our comparison sample. Our conclusions provide another "nail in the coffin" for assumptions that ULXs are simply a class of accreting IMBHs.

No other specific properties have been found for the ULX group, except for the spectral hardening at the highest luminosities. All these results suggests that ULXs are the highest luminosity end of stellar-mass BH binaries, with the largest BHs permitted by current formation mechanisms, and/or accreting at super-Eddington rates.

REFERENCES

Argyle, R. W., & Eldridge, P. 1990, MNRAS, 243, 504

Barnard, R., Kolb, U., & Osborne, J. P. 2003, A&A, 411, 553

Bauer, F. E., Brandt, W. N., Sambruna, R. M., Chartas, G., Garmire, G. P., Kaspi, S., & Netzer, H. 2001, AJ, 122, 182

Begelman, M. C. 2002, ApJ, 568, L97

Begelman, M. C., King, A. R., & Pringle, J. E. 2006, MNRAS, 370, 399

Belczynski, K., Sadowski, A., & Rasio, F. A. 2004, ApJ, 611, 1068

Bietenholz, M. F., Bartel, N., & Rupen, M. P. 2002, ApJ, 581, 1132

Bryant, J. J., & Hunstead, R. W. 1999, MNRAS, 308, 431

Clark, D. M., et al. 2005, ApJ, 631, L109

Colbert E., Heckman T., Ptak A., Strickland D., & Weaver K. A., 2004, ApJ, 602, 231

Colbert, E. J. M., & Mushotzky, R. F. 1999, ApJ, 519, 89

Colbert, E. J. M., Petre, R., Schlegel, E. M., & Ryder, S. D. 1995, ApJ, 446, 177

Colbert, E. J. M., & Ptak, A. F. 2002, ApJS, 143, 25

Cropper, M., Soria, R., Mushotzky, R. F., Wu, K., Markwardt, C. B., & Pakull, M. 2004, MNRAS, 349, 39

de Vaucouleurs, G., de Vaucouleurs, A., Corwin, H. G., Buta, R. J., Paturel, G., & Fouque, P. 1991, Third Reference Catalog of Bright Galaxies (RC3, New York: Springer-Verlag)

Done, C., & Kubota, A. 2006, MNRAS, 371, 1216

Dubus, G., & Rutledge, R. 2002, MNRAS, 336, 901

Eracleous, M., Shields, J. C., Chartas, G., & Moran, E. C. 2002, ApJ, 565, 108

Fabbiano, G., Zezas, A., & Murray, S. S. 2001, ApJ, 554, 1035

Fender, R., & Belloni, T. 2004, ARA&A, 42, 317

Feng, H., & Kaaret, P. 2005, ApJ, 633, 1052

Foschini, L., Rodriguez, J., Fuchs, Y., Ho, L. C., Dadina, M., Di Cocco, G., Courvoisier, T. J.-L., & Malaguti, G. 2004, A&A, 416, 529

Freeland, M., Kuncic, Z., Soria, R., & Bicknell, G. V. 2006, MNRAS, 372, 630

Gao, Y., Wang, Q. D., Appleton, P. N., & Lucas, R. A. 2003, ApJ, 596, L171

Ghosh, K. K., Finger, M. H., Swartz, D. A., Tennant, A. F., & Wu, K. 2006, ApJ, 640, 459

Goad, M. R., Roberts, T. P., Reeves, J. N., & Uttley, P. 2006, MNRAS, 365, 191

Gonçalves, A. C. & Soria R. 2006, MNRAS, 371, 673

Guainazzi, M., Matt, G., Brandt, W. N., Antonelli, L. A., Barr, P., & Bassani, L. 2000, A&A, 356, 463

Hasinger, G., Burg, R., Giacconi, R., Schmidt, M., Trumper, J., & Zamorani, G. 1998, A&A, 329, 482

Ho, L. C., Filippenko, A. V., & Sargent W. L. W. 1997, ApJS, 112, 315

Holt, S. S., Schlegel, E. M., Hwang, U., & Petre, R. 2003, ApJ, 588, 792

Humphrey, P. J., Fabbiano, G., Elvis, M., Church, M. J., & Balucinska-Church, M. 2003, MNRAS, 344, 134

Immler, S., Vogler, A., Ehle, M., & Pietsch, W. 1999, A&A, 352, 415

Jenkins, L. P., Roberts, T. P., Ward, M. J., & Zezas, A. 2004a, MNRAS, 352, 1335

Jenkins, L. P., Roberts, T. P., Warwick, R. S., Kilgard, R. E., & Ward, M. J. 2004b, MNRAS, 349, 404

Kaaret, P. 2002, ApJ, 578, 114

Kim, D.-W. et al. 2004, ApJ, 600, 59

King, A. R., & Pounds, K. A. 2003, MNRAS, 345, 657

King, A. R., Davies, M. B., Ward, M. J., Fabbiano, G., & Elvis, M. 2001, ApJ, 552, L109

Kong, A. K. H. 2003, MNRAS, 346, 265

Kong, A. K. H., & Di Stefano, R. 2005, ApJ, 632, L107

Kong, A. K. H., Garcia, M. R., Primini, F. A., Murray, S. S., Di Stefano, R., & McClintock, J. E. 2002, ApJ, 577, 738

Kraft, R. P., Kregenow, J. M., Forman, W. R., Jones, C., & Murray, S. S. 2001, ApJ, 560, 675

Kubota, A., Mizuno, T., Makishima, K., Fukazawa, Y., Kotoku, J., Ohnishi, T., & Tashiro, M. 2001, ApJ, 547, L119

Kubota, A., & Done, C. 2004, MNRAS, 353, 980

Kuntz, K. D., Gruendl, R. A.; Chu, Y.-H., Chen, C.-H. R., Still, M., Mukai, K., & Mushotzky, R. F. 2005, ApJ, 620, L31

La Parola, V., Damiani, F., Fabbiano, G., & Peres, G. 2003, ApJ, 583, L758

Lira, P., Lawrence, A., & Johnson, R. A. 2000, MNRAS, 319, 17

Lira, P., Ward, M., Zezas, A., Alonso-Herrero, A., & Ueno, S. 2002, MNRAS, 330, 259

Liu, J.-F., & Bregman, J. N. 2005, ApJS, 157, 59

Liu, Q. Z. & Mirabel, I. F., 2005, A&A, 429, 1125

Ma, C., et al. 1998, AJ, 116, 516

Matonick, D. M., & Fesen, R. A., 1997, ApJS, 112, 49

Matsumoto, H., Tsuru, T. G., Koyama, K., Awaki, H., Canizares, C. R., Kawai, N., Matsushita, S., & Kawabe, R. 2001, ApJ, 547, 25

McClintock J. E., & Remillard R. A., 2006, "Black Hole Binaries", in Compact Stellar X-ray Sources, eds. W.H.G. Lewin and M. van der Klis, Cambridge University Press, Cambridge

Miller, J. M., Fabian, A. C., & Miller, M. C. 2004, ApJ, 614, L117

Miller, J. M., Homan, J., Steeghs, D., Rupen, M., Hunstead, R. W., Wijnands, R., Charles, P. A., & Fabian, A. C. 2006, ApJ, 653, 525

Mucciarelli, P., Casella, P., Belloni, T., Zampieri, L., & Ranalli P. 2006, MNRAS, 365, 1123

Mukai, K., Pence, W. D., Snowden, S. L., & Kuntz, K. D. 2003, ApJ, 582, 184

Mukai K., Still M., Corbet R. H. D., Kuntz K. D., & Barnard R. 2005, ApJ, 634, 1085

Park, T., Kashyap, V. L., Siemiginowska, A., van Dyk, D. A., Zezas, A., Heinke, C., & Wargelin, B. J. 2006, ApJ, 652, 610

Pence, W. D., Snowden, S. L., Mukai, K., & Kuntz, K. D. 2001, ApJ, 561, 189

Pietsch, W. et al. 2001, A&A, 365, L174

Poutanen, J., Lipunova, G., Fabrika, S., Butkevich, A. G., & Abolmasov, P. 2007, MNRAS, 377, 1187

Primini, F. A., Forman, W., & Jones, C. 1993, ApJ, 410, 615

Protassov, R., van Dyk, D. A., Connors, A., Kashyap, V. L., & Siemiginowska, A. 2002, ApJ, 571, 545

Read, A. M. 2005, MNRAS, 359, 455

Read, A. M., Ponman, T. J., & Strickland, D. K. 1997, MNRAS, 286, 626

Revnivtsev, M., Sunyaev, R., Gilfanov, M., & Churazov, E. 2002, A&A, 385, 904

Roberts, T. P., 1997, PhD thesis, Univ. Leicester

Roberts, T. P., & Colbert, E. J. M. 2003, MNRAS, 341, L49

Roberts, T. P., Goad, M. R., Ward, M. J., & Warwick, R. S. 2003, MNRAS, 342, 709

Roberts, T. P., Goad, M. R., Ward, M. J., Warwick, R. S., O'Brien, P. T., Lira, P., & Hands, A. D. P. 2001, MNRAS, 325, L7

Roberts, T. P., & Warwick, R. S. 2000, MNRAS, 315, 98

Roberts, T. P., Warwick R. S., Ward M. J., & Goad M. R. 2004, MNRAS, 349, 1193

Roberts, T. P., Warwick, R. S., Ward, M. J., Goad, M. R., & Jenkins, L. P. 2005, MNRAS, 357, 1363

Roberts, T. P., Kilgard, R. E., Warwick, R. S., Goad, M. R., & Ward, M. J. 2006, MNRAS, 371, 1877

Roberts, T. P., Warwick, R. S., Ward, M. J., & Murray, S. S. 2002, MNRAS, 337, 677

Roberts, T. P. 2007, Ap&SS, 311, 203

Schlegel, E. M., Barrett, P., & Singh, K. P. 1997, AJ, 113, 1296

Schlegel, E. M., & Pannuti, T. G. 2003, AJ, 125, 3025

Smith, D. A., & Wilson, A. S. 2001, ApJ, 557, 180

Smith, D. A., & Wilson, A. S. 2003, ApJ, 591, 138

Soria, R., & Wu, K. 2003, A&A, 410, 53

Soria, R., & Wong, D. S. 2006, MNRAS, 372, 1531

Soria, R., Kuncic, Z., Broderick, J. W., & Ryder, S. D. 2006, MNRAS, 370, 1666

Soria, R., Baldi, A., Risaliti, G., Fabbiano, G., King, A., La Parola, V., & Zezas, A. 2007, MNRAS, 379, 1313

Stobbart, A.-M., Roberts, T. P., & Warwick, R. S. 2004, MNRAS, 351, 1063

Stobbart, A.-M., Roberts, T. P., & Warwick, R. S., 2006, MNRAS, 370, 25

Stobbart, A-M., Roberts, T. P., & Wilms, J. 2006, MNRAS, 368, 397

Strickland, D. K., Colbert, E. J. M., Heckman, T. M., Weaver, K. A., Dahlem, M., & Stevens, I. R. 2001, ApJ, 560, 707

Strohmayer, T. E., & Mushotzky, R. F. 2003, ApJ, 586, 61

Sugiho, M., Kotoku, J., Makishima, K., Kubota, A., Mizuno, T., Fukazawa, Y., & Tashiro, M. 2001, ApJ, 561, 73

Summers, L. K., Stevens, I. R., Strickland, D. K., & Heckman, T. M. 2003, MNRAS, 342, 690

Swartz, D. A., Ghosh, K. K., McCollough, M. L., Pannuti, T. G., Tennant, A. F., & Wu, K. 2003, ApJS, 144, 213

Swartz, D., Ghosh, K. Tennant, A., & Wu, K. 2004, ApJS, 154, 519

Tanaka, T., Sugiho, M., Kubota, A., Makishima, K., & Takahashi, T. 2005, PASJ, 57, 507

Tully, R. B. 1988, Nearby Galaxy Catalog (Cambridge)

van Dyk, D. A., Connors, A., Kashyap, V. L., & Siemiginowska, A. 2001, ApJ, 548, 224

Véron-Cetty, M.-P., & Véron, P. 2003, A&A, 412, 399

Vogler, A., & Pietsch, W. 1999, A&A, 342, 101

Vogler, A., Pietsch, W., & Bertoldi, F. 1997, A&A, 318, 768

Wang, Q. D. , Chaves, T., & Irwin, J. A. 2003, ApJ, 598, 969

Wang, Q. D., Immler, S., & Pietsch, W. 1999, ApJ, 523, 121

Weisskopf, M. C., et al. 2003, ExA, 16, 1

Weisskopf, M. C., Wu, K., Tennant, A. F., Swartz, D. A., & Ghosh, K. K. 2004, ApJ, 605, 360

Williams, B. F., Garcia, M. R., Kong, A. K. H., Primini, F. A., King, A. R., Di Stefano, R. & Murray, S. S. 2004, ApJ, 609, 735

Winter, L. M., Mushotzky, R. F., & Reynolds, C. S. 2006, ApJ, 649, 730

Wu, H., Xue, S. J., Xia, X. Y., Deng, Z. G., & Mao, S. 2002, ApJ, 576, 738

Zacharias, N., Urban, S. E., Zacharias, M. I., Wycoff, G. L., Hall, D. M., Monet, D. G., & Rafferty, T. J. 2004, AJ, 127, 3043

Zezas, A., Fabbiano, G., Rots, A. H., & Murray, S. S. 2002, ApJS, 142, 239

Table 1.   Piled-up observations

Obs. (1)	Name (2)	Position (3)	Galaxy (4)	Log L$_X$ (5)	OBSID (6)	Date (7)	CCD (8)	θ_{off} (9)	Count rate (10)	Reduced rate (11)	Pile-up (12)	Alternate names (13)	Ref (14)
							ULXs						
1	U5	X031820.0−662911	NGC 1313	39.47	2950	2002 Oct 13	7(1/1)	2.4	0.25	0.13	0.15		
2	-	X081929.0+704219	Holmberg II	39.91	1564	2001 Nov 02	7(1/4)	0.6	0.51	0.18	0.21	IXO 31, ULX1, X-1	1, 2, 3
3	U10	X095550.0+694046	M82	39.52	1302	1999 Sep 20	3(1/1)	0.4	0.12	0.12	0.14		
4	U10	X095550.0+694046		39.51	361	1999 Sep 20	3(1/1)	0.4	0.11	0.11	0.13		
5	U10	X095550.0+694046		40.11	379	2000 Mar 11	3(1/1)	4.2	0.46	0.09	0.11		
6	U36	X132938.6+582505	NGC 5204	39.85	2028	2001 Jan 09	7(1/8)	0.6	0.43	0.10	0.12		
7	-	X140319.6−412258	NGC 5408	39.82	2885	2002 May 07	7(1/4)	0.7	0.32	0.08	0.11	NGC 5408 X-1	4, 5, 6
8	U43	X141312.2−652014	Circinus	39.30	356	2000 Mar 14	7(1/1)	0.4	0.12	0.12	0.15		
							Comparison						
9	-	X095533.0+690033	M81	38.39	735	2000 May 07	7(1/1)	1.0	0.18	0.59	0.21	MF97	1, 4, 5, 6, 7

Note. — (1) Observation number; (2) Sample source name if the same as one in Table 2; (3) X-ray positions (J2000); (4) Host galaxy; (5) Approximate observed luminosity in units of erg s^{-1}, in the energy band 0.3−8.0 keV derived from the count rate of the reprocessed data; we assumed a power-law model with $\Gamma = 1.8$ and Galactic absorption column; (6) Observation ID; (7) Date of observation start; (8) CCD number where the object is located and subarray values (in parantheses); (9) Off axis angle of the source in arcmin; (10) Count rate in s^{-1}; (11) Reduced count rate calculated calculated for pile-up estimations explained in Section 2.4. This takes into account the off-axis angle in column 9 and the subarray values in column 8; (12) Pile-up estimation based on the reduced count rate in column 11; (13) Common names from the literature in column 14 (see Table 2 for common names and references for objects listed in column 2); (14) References.

References. — 1. Liu & Bregman (2005); 2. Colbert & Ptak (2002); 3. Goad et al. (2006); 4. Feng & Kaaret (2005); 5. Liu & Mirabel (2005); 6. Swartz et al. (2004); 7. Swartz et al. (2003);

Table 2. Properties of sample objects

No (1)	Name (2)	Position (3)	Galaxy (4)	Dist (5)	N_H^{Gal} (6)	OBS (7)	CCD (8)	Log L_X (9)	Date (10)	Exp (11)	Counts (12)	θ_{off} (13)	Alternate names (14)	Loc (15)	Ref (16)
									ULX sample						
1	U1	X012435.2+034731	NGC 520	29.6	3.3	2924	7(1/1)	40.1	2003 Jan 29	49.3	1037.2 ± 32.3	2.1	Source 11	DB	1
2	U2	X013350.9+303938	M33	0.7	5.69	787	7(1/4)	39.0	2000 Jan 11	9.3	26733.4 ± 163.6	8.9	M33 X-8	N	2, 3, 4, 5
3		X013350.9+303939			5.69	2023	7(1/1)	38.9	2001 Jul 06	88.8	171301.0 ± 415.2	12.5			
5	U3	X022231.4+422024	NGC 891	9.6	8.12	794	7(1/1)	39.4	2000 Nov 01	50.9	1977.4 ± 44.5	1.7	NGC 891 X-4	DB	6, 7
6	U4	X024238.9−000055	M77	15.2	3.54	344	7(1/1)	39.7	2000 Feb 21	47.4	1524.8 ± 39.6	0.7	-	A	8
7	U5	X031820.0−662911	NGC 1313	3.7	3.96	3550	2(1/1)	40.1	2002 Nov 09	14.6	10486.7 ± 102.7	6.0	IXO 7, XMM1, NGC 1313 X-1	B	9, 64, 10, 11
8	U6	X034555.7+680455	IC 342	3.9	29.39	2916	7(1/8)	39.5	2002 Apr 29	9.3	2033.6 ± 45.1	0.5	IXO 22, IC 342 X-7, XMM1, X-1	A	9, 12, 64, 6, 13, 26, 47
9		X034555.6+680456			29.39	2917	7(1/8)	39.5	2002 Aug 26	9.9	2191.8 ± 46.8	0.6			
10	U7	X073625.5+653540	NGC 2403	4.2	4.17	2014	7(1/1)	39.2	2001 Apr 17	35.6	5364.2 ± 73.3	2.7	Source 21, NGC 2403 X-1, XMM1	A	14, 6, 64
11	U8	X085333.7+511930	NGC 2681	13.3	2.48	2061	7(1/1)	39.2	2001 May 02	79.0	1105.9 ± 33.3	1.3	NGC 2681 PSX-3	D	15
12	U9	X095546.5+694040	M82	5.2	4.02	361	3(1/1)	39.0	1999 Sep 20	33.3	1174.2 ± 34.9	0.8	Source 9	SF	16
13	U10	X095550.1+694048			4.03	378	3(1/1)	40.0	1999 Dec 30	4.1	1404.7 ± 38.0	4.0	Source 7, M82 X-1	SF	16, 17, 29
14	U11	X095551.0+694045			4.03	2933	7(1/1)	39.2	2002 Jun 18	18.0	1595.2 ± 41.3	0.6	Source 5	SF	16
15	U12	X095551.1+694043			4.03	361	3(1/1)	39.1	1999 Sep 20	33.3	1353.6 ± 39.1	0.4	Source 4	SF	16
16	U13	X103843.3+533102	NGC 3310	18.7	1.12	2939	7(1/2)	39.7	2003 Jan 25	47.2	1003.9 ± 31.7	0.3	IXO 38, NGC 3310 ULX2, X-3	A	9, 18, 19
17	U14	X103845.9+533012			1.11	2939	7(1/2)	39.8	2003 Jan 25	47.2	1541.8 ± 41.0	0.6	NGC 3310 X-1, X1	N	6, 18
18	U15	X103846.0+533004			1.11	2939	7(1/2)	39.8	2003 Jan 25	47.2	1221.6 ± 35.7	0.7	-	SF	-
19	U16	X111126.0+554017	M108	14.1	0.78	2025	7(1/1)	39.4	2001 Sep 08	59.4	1278.9 ± 35.9	2.8	Source 26	D	20
20	U17	X112015.8+133514	NGC 3628	7.7	2.22	2039	7(1/1)	39.3	2000 Dec 02	58.0	2995.8 ± 54.8	0.9	IXO 39	DB	9, 21
21	U18	X120151.4−185225	NGC 4038/9	21.7	3.95	3040	7(1/1)	39.7	2001 Dec 29	69.0	1009.7 ± 31.9	0.9	Source 11	AM	22, 23
22		X120151.3−185225			3.95	3043	7(1/1)	39.8	2002 Apr 18	67.1	1377.4 ± 37.3	1.0			
23		X120151.3−185225			3.95	3041	7(1/1)	39.8	2002 Nov 22	72.9	1491.4 ± 38.8	0.9			
24	U19	X120152.1−185134			3.95	315	7(1/1)	39.9	1999 Dec 01	72.2	1984.1 ± 44.6	1.6	Source 16	AM	22, 23
25		X120152.1−185133			3.95	3040	7(1/1)	39.8	2001 Dec 29	69.0	1587.0 ± 40.0	0.9			
26		X120152.1−185133			3.95	3042	7(1/1)	39.8	2002 May 31	67.3	1474.9 ± 38.5	1.6			
27		X120152.1−185133			3.95	3041	7(1/1)	39.8	2002 Nov 22	72.9	1491.8 ± 38.8	0.8			
28	U20	X120155.6−185215			3.96	315	7(1/1)	39.8	1999 Dec 01	72.2	1344.0 ± 37.3	1.9	Source 42	AM	22, 23
29	U21	X120156.4−185158			3.96	315	7(1/1)	39.7	1999 Dec 01	72.2	1307.1 ± 36.2	1.6	Source 44	AM	22, 23
30		X120156.5−185157			3.96	3040	7(1/1)	39.7	2001 Dec 29	69.0	1264.8 ± 35.6	0.4			
31	U22	X120807.5+651028	NGC 4125	18.1	1.82	2071	7(1/1)	39.5	2001 Sep 09	64.2	1051.7 ± 33.0	0.4	-	E	68
32	U23	X123030.6+414142	NGC 4485	9.3	1.78	1579	7(1/1)	39.6	2000 Nov 03	19.5	1450.1 ± 38.1	2.6	IXO 62, NGC 4485 X-1	A	9, 6, 24
33	U24	X123049.2+122604	M87	17.1	2.54	2707	7(1/1)	39.3	2002 Jul 06	98.7	1064.6 ± 36.8	3.1	-	E	68
34	U25	X123551.7+275604	NGC 4559	9.7	0.82	2026	7(1/4)	39.9	2001 Jan 14	9.4	1434.4 ± 37.9	0.6	IXO 65, NGC 4559 X-1, X7	D	9, 6, 25, 26, 48
35		X123551.7+275604			0.82	2027	7(1/4)	40.1	2001 Jun 04	10.7	2093.2 ± 45.8	0.6			
36	U26	X123558.6+275742			0.8	2027	7(1/4)	39.8	2001 Jun 04	10.7	1300.9 ± 36.1	2.9	IXO 66, NGC 4559 X-4, X10	DB	9, 6, 25, 26, 48
37	U27	X123617.4+255856	NGC 4565	16.4	1.31	3950	7(1/1)	39.8	2003 Feb 08	59.2	2146.5 ± 46.5	2.0	IXO 67, NGC 4565 ULX4	B	9, 27, 28
38	U28	X123740.3+114728	NGC 4579	20.3	2.52	807	7(1/4)	40.1	2000 May 02	33.9	1654.6 ± 40.7	1.3	NGC 4579 X-1	D	30
39	U29	X124155.6+323217	NGC 4631	6.9	1.29	797	7(1/1)	39.2	2000 Apr 16	59.2	3223.1 ± 56.8	0.5	IXO 66, NGC 4631 X-1, XMM1	SF	9, 6, 64
40	U30	X125053.3+410714	M94	4.3	1.44	808	7(1/4)	39.0	2000 May 13	47.4	4472.6 ± 70.8	0.7	NGC 4736 X-1	DB	30
41	U31	X130521.9−492827	NGC 4945	5.2	14.94	864	7(1/1)	39.1	2000 Jan 27	49.1	2983.5 ± 54.9	1.3	NGC 4945 XMM4	DB	64
42	U32	X130532.9−492734			14.84	864	7(1/1)	39.1	2000 Jan 27	49.1	2797.7 ± 53.2	0.7	NGC 4945 X-2, XMM1	DB	31, 64
43	U33	X131519.5+420302	NGC 5055	7.2	1.3	2197	7(1/1)	39.8	2001 Aug 27	28.0	2354.6 ± 48.6	6.0	IXO 74, NGC 5055 X-2	D	9, 6
44	U34	X132507.4−430410	Cen A	4.9	8.41	316	3(1/1)	39.0	1999 Dec 05	35.7	1108.8 ± 33.9	9.2	IXO 75	E	9, 32
45		X132507.5−430410			8.41	962	1(1/1)	39.3	2000 May 17	36.5	2556.1 ± 50.7	5.5			
46	U35	X132519.8−430317			8.4	316	3(1/1)	39.2	1999 Dec 05	35.7	2124.0 ± 46.4	7.1	IXO 76	E	9, 32, 63
47	U36	X132938.6+582506	NGC 5204	4.8	1.38	2029	7(1/8)	39.4	2001 May 02	9.0	1498.1 ± 38.7	0.6	IXO 77, NGC 5204 X-1, XMM1	SF	9, (6, 18, 26, 33, 34), 64
48	U37	X133719.8−295349	M83	4.7	3.69	793	6(1/1)	39.0	2000 Apr 29	51.0	2419.2 ± 49.2	2.7	IXO 82, H30, XMM1	D	9, 35, 64
49	U38	X140304.0+542735	M101	5.4	1.15	4731	6(1/1)	39.2	2004 Jan 19	56.2	3213.5 ± 56.8	4.4	MF37, ULX2, H19, XMM-1, XMM2	A	39, 18, 37, 40, 64
50	U39	X140314.3+541806			1.15	5309	7(1/1)	39.0	2004 Mar 14	70.8	3889.1 ± 62.6	5.2	H25, P51, XMM-2, XMM1	A	37, 38, 40, 64

Table 2—Continued

No (1)	Name (2)	Position (3)	Galaxy (4)	Dist (5)	N_H^{Gal} (6)	OBS (7)	CCD (8)	Log L_X (9)	Date (10)	Exp (11)	Counts (12)	θ_{off} (13)	Alternate names (14)	Loc (15)	Ref (16)
51		X140314.3+541806			1.15	4732	7(1/1)	39.0	2004 Mar 19	69.8	3902.9 ± 62.8	5.2			
52	U40	X140332.4+542103			1.15	934	7(1/1)	39.2	2000 Mar 26	98.2	9024.5 ± 95.1	3.8	M101 X5, H32, P98, ULX-1	A	18, 37, 38, 49, 65, 66, 60
53	U41	X140414.3+542604			1.15	934	3(1/1)	39.1	2000 Mar 26	98.2	3549.6 ± 59.7	10.6	IXO 83, ULX3, H45, XMM-3	D	9, 18, 37, 40
54		X140414.1+542603			1.15	4731	2(1/1)	38.8	2004 Jan 19	56.2	1085.5 ± 33.1	8.7			
55		X140414.2+542603			1.15	5300	3(1/1)	39.2	2004 Mar 07	52.1	2306.5 ± 48.2	11.0			
56		X140414.2+542603			1.15	5309	3(1/1)	38.9	2004 Mar 14	70.8	1592.2 ± 40.2	11.5			
57		X140414.2+542603			1.15	4732	3(1/1)	38.8	2004 Mar 19	69.8	1147.7 ± 34.3	11.5			
58	U42	X141310.1−652045	Circinus	3.7	59.7	356	7(1/1)	39.1	2000 Mar 14	23.1	1715.3 ± 41.4	0.9	CG X-2, source F	D	41, 42
59	U43	X141312.2−652014			59.92	365	7(1/8)	39.7	2000 Mar 14	5.0	1634.5 ± 40.5	0.4	CG X-1, source J	D	41, 42, 43
60	U44	X145358.9+033217	NGC 5775	22.4	3.51	2940	7(1/1)	39.9	2002 Apr 05	58.2	1324.2 ± 36.4	1.1	-	D	
61	U45	X203500.7+601131	NGC 6946	5.5	20.23	1043	7(1/1)	39.6	2001 Sep 07	58.3	8451.9 ± 92.1	4.8	MF16, NGC 6946 X-11, 58, X8	D	44, 6, 45, 46
62		X203500.8+601131			20.23	4404	7(1/1)	39.5	2002 Nov 25	30.0	3750.0 ± 61.3	2.9			
63	U46	X225724.7−410344	NGC 7424	11.5	1.33	3496	7(1/1)	39.7	2002 Jun 11	23.9	1370.8 ± 37.0	2.2	ULX2	A	67
64	U47	X225728.9−410212			1.32	3496	7(1/1)	39.7	2002 Jun 11	23.9	1331.9 ± 36.5	0.5	ULX1	D	67
						Comparison sample									
1	C1	X001528.9−391319	NGC 55	1.3	1.74	2255	0(1/1)	38.43	2001 Sep 11	59.4	8553.3 ± 92.5	3.7	Source 7, 6, N55	D	50, 7, 51, 52
2	C2	X004238.5+411604	M31	0.7	6.66	1585	0(1/1)	38.30	2001 Nov 19	4.9	1806.5 ± 42.6	4.9	r2-26, source 35	DB	(53, 62), (54, 55, 56)
3		X004238.5+411604			6.66	2895	0(1/1)	38.39	2001 Dec 07	4.9	2130.6 ± 46.3	5.3			
4		X004238.6+411603			6.66	2896	1(1/1)	38.40	2002 Feb 06	4.9	2302.4 ± 48.1	5.2			
5		X004238.6+411604			6.66	2898	3(1/1)	38.48	2002 Jun 02	4.9	2384.3 ± 49.0	6.8			
6	C3	X004305.7+411703			6.74	1575	7(1/1)	38.27	2001 Oct 05	37.7	20560.8 ± 143.5	4.8	-	DB	62, 55
7	C4	X004722.6−252051	NGC 253	3.0	1.35	790	6(1/1)	38.36	1999 Dec 27	43.5	1022.2 ± 32.3	7.8	NGC 253 PSX-5, X21, XMM2	A	15, (57, 58, 61), 64
8	C5	X004733.0−251749			1.37	969	7(1/1)	38.67	1999 Dec 16	14.0	1150.2 ± 34.0	0.3	NGC 253 PSX-2, X33, XMM1		15, (57, 58), 64
9		X004733.0−251749			1.37	790	7(1/1)	38.85	1999 Dec 27	43.5	3246.7 ± 57.4	5.5			
10	C6	X004735.2−251512			1.39	790	6(1/1)	38.57	1999 Dec 27	43.5	1811.8 ± 42.6	3.8	NGC253 PSX-7, X36, XMM3	A	15, (57, 58), 64
11	C7	X073655.6+653541	NGC 2403	4.2	4.17	2014	7(1/1)	38.94	2001 Apr 17	35.6	2608.9 ± 51.1	1.1	Source 20, XMM3	DB	14, 64
12	C8	X073702.4+653935			4.18	2014	7(1/1)	38.72	2001 Apr 17	35.6	1600.1 ± 40.1	5.0	Source 1, NGC 2403 X-4, XMM4	A	14, 6, 64
13	C9	X122809.3+440508	NGC 4449	3.0	1.5	2031	7(1/1)	38.38	2001 Feb 04	26.6	1138.8 ± 33.8	2.3	NGC 4449 X-1, source 10	SF	6, 59
14	C10	X122817.8+440634			1.49	2031	7(1/1)	38.46	2001 Feb 04	26.6	1356.9 ± 36.9	1.7	NGC 4449 X-7, source 27	SF	6, 59
15	C11	X124211.1+323236	NGC 4631	6.9	1.29	797	7(1/1)	38.73	2000 Apr 16	59.2	1104.0 ± 33.3	3.1	NGC 4631 PSX-1, XMM5	D	15, 64
16	C12	X125050.3+410712	M94	4.3	1.44	808	7(1/4)	38.51	2000 May 13	47.4	1349.6 ± 37.0	0.3	M94 X-4	DB	30
17	C13	X125052.7+410719			1.44	808	7(1/4)	38.79	2000 May 13	47.4	2553.3 ± 51.6	0.6	M94 X-3	DB	30
18	C14	X125053.1+410712			1.44	808	7(1/4)	38.83	2000 May 13	47.4	2782.9 ± 53.6	0.6	M94 X-2	DB	30
19	C15	X130518.5−492824	NGC 4945	5.2	14.96	864	7(1/1)	38.69	2000 Jan 27	49.1	1115.3 ± 33.8	1.8	NGC 4945 XMM3	DB	64
20	C16	X130538.1−492545			14.74	864	6(1/1)	38.94	2000 Jan 27	49.1	1535.9 ± 39.3	2.6	Source 3, NGC 4945 XMM2	D	31, 64
21	C17	X133659.5−294959	M83	4.7	3.69	793	7(1/1)	38.54	2000 Apr 29	51.0	1249.9 ± 35.5	3.9	H17, source 28, M83 XMM2	A	35, 36, 64
22	C18	X133700.9−295203			3.7	793	7(1/1)	38.58	2000 Apr 29	51.0	1341.9 ± 40.8	2.0	source 44	DB	36
23	C19	X133704.3−295404			3.72	793	7(1/1)	38.59	2000 Apr 29	51.0	1381.1 ± 37.2	1.0	H26, source 62	A	35, 36
24	C20	X133704.4−295122			3.69	793	7(1/1)	38.63	2000 Apr 29	51.0	1527.7 ± 39.2	2.2	H27, source 64, M83 XMM3	DB	35, 36, 64
25	C21	X140228.3+541627	M101	5.4	1.14	5322	6(1/1)	38.76	2004 May 03	64.7	1235.2 ± 35.3	5.6	M101 XMM4	D	64
26	C22	X203500.1+600908	NGC 6946	5.5	20.13	1043	7(1/1)	38.91	2001 Sep 07	58.3	1894.7 ± 43.6	3.4	IXO 85, NGC 6946 X-9, 56, X7	A	9, 6, 45, 46

Note. — (1) Observation number; (2) Source name; (3) X-ray positions (J2000); (4) Host galaxy; (5) Galaxy distance from Tully(1988) in Mpc; (6) Galactic absorption column in units of 10^{20}cm^{-2}; (7) Observation ID; (8) CCD number where the object is located and subarray values (in parantheses). The subarray value represents the fraction of the CCD actually used in the observation; (9) Approximate observed luminosity in units of erg s^{-1}, in the energy band 0.3−8.0 keV derived from the count rate of the reprocessed data; we assumed a power-law model with $\Gamma = 1.8$ and Galactic absorption column; (10) Date of observation start; (11) Exposure time in ks; (12) Net counts in the 0.3−8.0 keV energy band; (13) Off axis angle of the source in arcmin. The values listed here and the subarray values in column 8 were used when we rejected the piled-up sources; (14) Common names from the literature in column 16 (the names correspond to references in the same order; references

that use the same name are in parantheses; some papers do not give special names or the names are given using the coordinates, these were not used); (15) Location in the galaxy; abbreviations are: A - spiral arm, D - disk, DB - disk or bulge, E - elliptical galaxy, no special location, SF - star forming region, AM - arm in merger, N - nucleus; (16) References

References. — 1. Read (2005); 2. Dubus & Rutledge (2002); 3. Colbert & Mushotzky (1999); 4. Foschini et al. (2004); 5. La Parola et al. (2003); 6. Roberts & Warwick (2000); 7. Read, Ponman, & Strickland (1997); 8. Smith & Wilson (2003); 9. Colbert & Ptak (2002); 10. Colbert et al. (1995); 11. Miller, Fabian & Miller (2004); 12. Kong (2003); 13. Sugiho et al. (2001); 14. Schlegel & Pannuti (2003); 15. Humphrey et al. (2003); 16. Matsumoto et al. (2001); 17. Strohmayer & Mushotzky (2003); 18. Liu & Bregman (2005); 19. Jenkins et al. (2004a); 20. Wang, Chaves & Irwin (2003); 21. Strickland et al. (2001); 22. Fabbiano, Zezas & Murray (2001); 23. Zezas et al. (2002); 24. Roberts et al. (2002); 25. Vogler, Pietsch & Bertoldi (1997); 26. Roberts et al. (2004); 27. Foschini et al. (2004); 28. Wu et al. (2002); 29. Mucciarelli et al. (2006); 30. Eracleous et al. (2002); 31. Guainazzi et al. (2000); 32. Kraft et al. (2001); 33. Roberts et al. (2001); 34. Roberts et al. (2005); 35. Immler et al. (1999); 36. Soria & Wu (2003); 37. Wang, Immler & Pietsch (1999); 38. Pence et al. (2001); 39. Matonick, & Fesen (1997); 40. Jenkins et al. (2004b); 41. Bauer et al. (2001); 42. Smith & Wilson (2001); 43. Weisskopf et al. (2004); 44. Roberts & Colbert (2003); 45. Holt et al. (2003); 46. Lira, Lawrence & Johnson (2000); 47. Roberts et al. (2003); 48. Cropper et al. (2004); 49. Mukai et al. (2003); 50. Schlegel, Barrett & Singh (1997); 51. Roberts (1997); 52. Stobbart, Roberts & Warwick (2004); 53. Kong et al. (2002); 54. Primini, Forman & Jones (1993); 55. Kaaret (2002); 56. Barnard, Kolb & Osborne (2003); 57. Vogler & Pietsch (1999); 58. Pietsch et al. (2001); 59. Summers et al. (2003); 60. Kuntz et al. (2005); 61. Tanaka et al. (2005); 62. Williams et al. (2004); 63. Ghosh et al. (2006); 64. Winter, Mushotzky & Reynolds (2006); 65. Mukai et al. (2005); 66. Kong & Di Stefano (2005); 67. Soria et al. (2006); 68. Swartz et al. (2004);

Table 3. Single-component spectral fits

		PL model[a]				MCD model[a]				
Source	Γ^b	N_H^f	Norm PL[d]	Good fits[h]	$\chi^2/$d.o.f.[g]	kT_{in}^c	N_H^f	Norm MCD[e]	Good fits[h]	$\chi^2/$d.o.f.[g]
		$(10^{21}$ cm$^{-2})$			(keV)		$(10^{21}$ cm$^{-2})$			
(1)	(2)	(3)	(4)	(5)	(6)	(7)	(8)	(9)	(10)	(11)
ULX sample										
U1	$2.56^{+0.23}_{-0.21}$	$4.8^{+0.8}_{-0.7}$	$7.8^{+12.0}_{-1.4}\times10^{-5}$		68.6/53	$0.91^{+0.11}_{-0.10}$	$2.0^{+0.5}_{-0.4}$	$1.1^{+0.8}_{-0.4}\times10^{-2}$		95.5/53
U2	2.11	2.4	5.5		2296.5/728	1.07	0.7	6.4		2792.4/728
U3	$1.94^{+0.14}_{-0.13}$	$7.6^{+0.9}_{-0.8}$	$1.4^{+1.0}_{-0.2}\times10^{-4}$		70.0/100	$1.43^{+0.14}_{-0.12}$	4.8 ± 0.5	$5.9^{+2.4}_{-1.7}\times10^{-3}$	G	91.8/100
U4	$0.81^{+0.14}_{-0.13}$	$5.3^{+1.2}_{-1.0}$	$3.8^{+10.3}_{-0.6}\times10^{-5}$	G	93.1/86	(>3.61)	$5.6^{+0.8}_{-0.7}$	$1.9^{+2.7}_{-0.1}\times10^{-4}$	G	94.7/86
U5	1.70 ± 0.05	4.5 ± 0.3	$2.2^{+0.2}_{-0.1}\times10^{-3}$	G	304.7/289	$1.66^{+0.07}_{-0.06}$	2.5 ± 0.2	$6.9^{+1.1}_{-0.9}\times10^{-2}$		353.6/289
U6	1.71 ± 0.09	3.7 ± 0.5	$6.0^{+0.7}_{-0.6}\times10^{-4}$	G	215.7/215	$1.71^{+0.13}_{-0.12}$	1.3 ± 0.3	$1.6^{+0.5}_{-0.4}\times10^{-2}$		259.8/215
U7	2.17 ± 0.07	4.2 ± 0.3	$4.4^{+0.8}_{-0.3}\times10^{-4}$		260.3/182	$1.13^{+0.05}_{-0.04}$	2.1 ± 0.2	$3.9^{+0.7}_{-0.6}\times10^{-2}$	G	172.6/182
U8	$1.88^{+0.16}_{-0.15}$	1.7 ± 0.4	$2.3^{+8.1}_{-0.3}\times10^{-5}$	G	60.8/58	$1.21^{+0.13}_{-0.12}$	0.3 ± 0.2	$2.1^{+0.9}_{-0.7}\times10^{-3}$	G	53.4/58
U9	$2.45^{+0.22}_{-0.20}$	$7.0^{+1.3}_{-1.2}$	$2.0^{+1.6}_{-0.4}\times10^{-4}$	G	63.7/61	$1.11^{+0.12}_{-0.11}$	3.0 ± 0.8	$1.3^{+0.7}_{-0.5}\times10^{-2}$		76.7/61
U10	$1.00^{+0.21}_{-0.20}$	$10.5^{+2.7}_{-2.4}$	$7.3^{+3.8}_{-1.9}\times10^{-4}$	G	72.0/81	>3.42	$9.3^{+1.2}_{-1.1}$	<6.8	G	77.4/81
U11	$1.16^{+0.25}_{-0.23}$	$30.3^{+5.1}_{-4.4}$	$3.2^{+3.0}_{-1.0}\times10^{-4}$	G	82.8/96	>3.23	$26.6^{+2.3}_{-2.1}$	$9.6^{+0.7}_{-0.5}\times10^{-4}$	G	87.9/96
U12	$2.81^{+0.71}_{-0.63}$	$225.7^{+45.3}_{-38.8}$	$7.7^{+21.1}_{-5.3}\times10^{-3}$	G	99.8/84	$1.89^{+0.58}_{-0.37}$	$179.2^{+30.5}_{-26.6}$	$2.1^{+4.2}_{-1.5}\times10^{-2}$		101.8/84
U13	$2.52^{+0.27}_{-0.23}$	$2.3^{+0.5}_{-0.4}$	$4.4^{+10.8}_{-0.6}\times10^{-5}$		69.9/50	$0.81^{+0.12}_{-0.11}$	$0.3^{+0.3}_{-0.2}$	$1.1^{+0.9}_{-0.5}\times10^{-2}$		100.8/50
U14	$1.46^{+0.16}_{-0.14}$	$5.1^{+1.0}_{-0.9}$	$6.6^{+10.2}_{-1.0}\times10^{-5}$	G	80.9/88	$2.07^{+0.34}_{-0.26}$	$3.3^{+0.6}_{-0.5}$	$1.2^{+0.8}_{-0.5}\times10^{-3}$	G	87.2/88
U15	$1.78^{+0.18}_{-0.16}$	$6.5^{+1.3}_{-1.1}$	$7.3^{+12.9}_{-1.4}\times10^{-5}$	G	76.8/70	$1.53^{+0.19}_{-0.16}$	$4.2^{+0.8}_{-0.7}$	$2.8^{+1.5}_{-1.0}\times10^{-3}$	G	66.7/70
U16	$1.90^{+0.16}_{-0.15}$	$3.9^{+0.6}_{-0.5}$	$5.0^{+8.7}_{-0.7}\times10^{-5}$	G	73.1/65	$1.30^{+0.14}_{-0.12}$	$2.1^{+0.4}_{-0.3}$	$3.2^{+1.4}_{-1.0}\times10^{-3}$	G	65.9/65
U17	1.71 ± 0.11	7.6 ± 0.7	$1.5^{+0.9}_{-0.2}\times10^{-4}$	G	149.7/149	$1.69^{+0.15}_{-0.14}$	$5.2^{+0.5}_{-0.4}$	$4.4^{+1.6}_{-1.2}\times10^{-3}$		182.6/149
U18	1.79 ± 0.08	$4.0^{+0.3}_{-0.4}$	$4.7\pm0.4\times10^{-5}$		270.2/208	$1.48^{+0.10}_{-0.09}$	2.1 ± 0.2	$2.1^{+0.5}_{-0.4}\times10^{-3}$		269.4/208
U19	$1.15^{+0.05}_{-0.02}$	0.6 ± 0.1	$2.2^{+0.2}_{-0.1}\times10^{-5}$	G	391.6/345	$2.65^{+0.21}_{-0.22}$	<0.1	$2.6^{+0.8}_{-0.5}\times10^{-4}$		416.7/345
U20	$1.22^{+0.13}_{-0.11}$	$0.2(<0.5)$	$1.8^{+6.8}_{-0.2}\times10^{-5}$	G	62.2/75	$1.89^{+0.26}_{-0.24}$	<0.1	$6.1^{+4.0}_{-2.0}\times10^{-4}$	G	84.6/75
U21	$1.97^{+0.11}_{-0.10}$	$1.4^{+0.3}_{-0.1}$	$2.8\pm0.2\times10^{-5}$		203.7/133	1.16 ± 0.08	<0.2	$2.8^{+0.3}_{-0.6}\times10^{-3}$		211.1/133
U22	$2.00^{+0.19}_{-0.17}$	0.7 ± 0.3	$2.1^{+7.9}_{-0.3}\times10^{-5}$	G	48.5/53	$0.79^{+0.09}_{-0.08}$	<0.1	$9.0^{+4.3}_{-2.9}\times10^{-3}$		84.3/53
U23	$1.80^{+0.14}_{-0.13}$	3.4 ± 0.5	$1.5^{+1.0}_{-0.2}\times10^{-4}$		97.8/75	$1.41^{+0.14}_{-0.12}$	$1.7^{+0.4}_{-0.3}$	$8.3^{+3.3}_{-2.4}\times10^{-3}$	G	80.5/75
U24	$2.52^{+0.28}_{-0.25}$	$1.9^{+0.5}_{-0.4}$	$2.1^{+9.6}_{-0.3}\times10^{-5}$	G	59.1/66	$0.73^{+0.10}_{-0.09}$	0.3 ± 0.2	$8.3^{+5.8}_{-3.2}\times10^{-3}$	G	70.4/66
U25	$2.25^{+0.11}_{-0.10}$	1.6 ± 0.2	$2.5\pm0.2\times10^{-4}$		252.3/169	0.91	0.1	5.0		361.5/169
U26	$1.89^{+0.14}_{-0.13}$	2.5 ± 0.4	$2.2^{+1.1}_{-0.3}\times10^{-4}$	G	70.1/67	$1.29^{+0.13}_{-0.11}$	$1.0^{+0.3}_{-0.2}$	$1.6^{+0.6}_{-0.4}\times10^{-2}$	G	56.8/67
U27	2.00 ± 0.12	3.5 ± 0.4	$8.3^{+7.0}_{-0.9}\times10^{-5}$	G	119.4/108	$1.20^{+0.10}_{-0.09}$	1.7 ± 0.2	$6.8^{+2.3}_{-1.7}\times10^{-3}$		134.6/108
U28	1.88 ± 0.12	1.7 ± 0.3	$7.8^{+7.3}_{-0.8}\times10^{-5}$	G	82.8/83	$1.33^{+0.12}_{-0.11}$	0.3 ± 0.2	$5.1^{+1.9}_{-1.4}\times10^{-3}$	G	79.4/83
U29	1.90 ± 0.09	$2.7^{+0.3}_{-0.2}$	$1.0^{+0.6}_{-0.1}\times10^{-4}$	G	158.7/135	$1.28^{+0.09}_{-0.08}$	$1.1^{+0.2}_{-0.1}$	$7.3^{+2.0}_{-1.6}\times10^{-3}$		204.2/135
U30	$1.26^{+0.07}_{-0.06}$	0.2 ± 0.1	$8.6^{+4.2}_{-0.5}\times10^{-5}$	G	166.7/184	$1.86^{+0.17}_{-0.12}$	<0.1	$3.0^{+0.8}_{-0.7}\times10^{-3}$		265.5/184
U31	$2.27^{+0.11}_{-0.10}$	$5.7^{+0.6}_{-0.5}$	$2.5^{+1.0}_{-0.3}\times10^{-4}$		188.8/142	1.13 ± 0.06	$2.9^{+0.4}_{-0.3}$	$1.9^{+0.5}_{-0.4}\times10^{-2}$	G	154.9/142
U32	1.79 ± 0.11	$6.4^{+0.8}_{-0.7}$	$1.8^{+1.0}_{-0.2}\times10^{-4}$	G	158.9/142	$1.60^{+0.13}_{-0.12}$	$3.9^{+0.5}_{-0.4}$	$5.6^{+1.8}_{-1.4}\times10^{-3}$	G	153.1/142
U33	$2.50^{+0.14}_{-0.13}$	2.6 ± 0.3	$4.7^{+1.1}_{-0.5}\times10^{-4}$		131.5/104	0.80 ± 0.06	0.7 ± 0.2	$1.3^{+0.5}_{-0.3}\times10^{-1}$		179.1/104
U34	3.97	2.9	1.7		514.9/148	0.26	1.5	6.3		611.5/148
U35	$2.42^{+0.14}_{-0.13}$	2.6 ± 0.5	$2.3^{+1.0}_{-0.3}\times10^{-4}$	G	93.9/103	0.95 ± 0.06	$0.2(<0.5)$	$3.3^{+1.0}_{-0.8}\times10^{-2}$	G	84.2/103
U36	$3.11^{+0.22}_{-0.20}$	2.0 ± 0.3	$3.3^{+1.2}_{-0.3}\times10^{-4}$	G	63.8/70	0.49 ± 0.05	$0.3^{+0.2}_{-0.1}$	$5.6^{+3.1}_{-1.9}\times10^{-1}$		105.2/70
U37	2.43 ± 0.12	$1.9^{+0.4}_{-0.3}$	$1.3^{+0.8}_{-0.1}\times10^{-4}$		150.6/106	0.90 ± 0.05	<0.1	$2.4^{+0.5}_{-0.4}\times10^{-2}$		154.7/106
U38	1.86 ± 0.09	3.5 ± 0.4	$1.5^{+0.7}_{-0.1}\times10^{-4}$	G	178.8/151	$1.46^{+0.09}_{-0.08}$	$1.5^{+0.3}_{-0.2}$	$6.8^{+1.7}_{-1.3}\times10^{-3}$	G	149.1/151
U39	$2.17^{+0.08}_{-0.07}$	1.9 ± 0.1	$1.0\pm0.1\times10^{-4}$		430.4/282	0.91	0.5	2.1		800.3/282
U40	$6.51^{+0.27}_{-0.22}$	3.9 ± 0.3	$1.9^{+0.4}_{-0.1}\times10^{-4}$		315.6/84	0.16 ± 0.01	1.3 ± 0.1	$1.2^{+0.4}_{-0.3}\times10^2$		257.2/84
U41	$3.49^{+0.04}_{-0.09}$	$4.2^{+0.1}_{-0.2}$	$1.2\pm0.1\times10^{-4}$	G	466.7/399	0.57 ± 0.02	0.9 ± 0.1	$7.4^{+1.4}_{-1.1}\times10^{-2}$		576.8/399

Table 3—Continued

	PL model[a]					MCD model[a]				
Source	Γ^b	N_H^f	Norm PL[d]	Good fits[h]	$\chi^2/$ d.o.f.[g]	kT_{in}^c	N_H^f	Norm MCD[e]	Good fits[h]	$\chi^2/$ d.o.f.[g]
		$(10^{21}$ cm$^{-2})$			(keV)	$(10^{21}$ cm$^{-2})$				
(1)	(2)	(3)	(4)	(5)	(6)	(7)	(8)	(9)	(10)	(11)
U42	$1.48^{+0.17}_{-0.16}$	$4.7^{+1.6}_{-1.4}$	$2.1^{+1.6}_{-0.4}\times10^{-4}$		133.0/93	$2.25^{+0.40}_{-0.31}$	$2.0^{+1.0}_{-0.9}$	$2.8^{+1.9}_{-1.2}\times10^{-3}$		140.7/93
U43	$1.46^{+0.17}_{-0.16}$	$5.3^{+1.7}_{-1.5}$	$1.0^{+0.3}_{-0.2}\times10^{-3}$	G	76.8/87	$2.36^{+0.42}_{-0.31}$	$2.4^{+1.1}_{-1.0}$	$1.2^{+0.7}_{-0.5}\times10^{-2}$	G	76.2/87
U44	$1.90^{+0.26}_{-0.24}$	$29.6^{+4.4}_{-3.9}$	$2.0^{+2.4}_{-0.6}\times10^{-4}$	G	84.9/75	$1.96^{+0.32}_{-0.26}$	$22.0^{+2.7}_{-2.4}$	$2.3^{+1.7}_{-1.0}\times10^{-3}$	G	82.9/75
U45	2.60	1.3	3.9		729.9/321	0.61	0.0	3.3		1436.3/321
U46	$2.29^{+0.18}_{-0.16}$	2.1±0.4	$1.1^{+1.0}_{-0.1}\times10^{-4}$	G	67.4/66	0.92±0.10	0.3±0.2	$2.0^{+1.0}_{-0.7}\times10^{-2}$		99.4/66
U47	1.80±0.14	2.3±0.4	$10.0^{+8.5}_{-1.2}\times10^{-5}$	G	62.5/70	$1.29^{+0.14}_{-0.12}$	0.9±0.2	$7.4^{+3.3}_{-2.3}\times10^{-3}$	G	69.9/70
Comparison sample										
C1	$3.69^{+0.10}_{-0.09}$	4.7±0.2	$10.0^{+1.1}_{-0.6}\times10^{-4}$		377.3/157	0.55±0.02	1.3±0.1	$6.4^{+1.3}_{-1.0}\times10^{-1}$		561.5/157
C2	1.49±0.05	$1.3^{+0.3}_{-0.2}$	$8.1^{+0.6}_{-0.5}\times10^{-4}$		590.0/447	1.86±0.08	< 0.1	$2.2\pm0.3\times10^{-2}$		560.6/447
C3	2.85±0.04	2.5±0.1	$1.5^{+0.1}_{-0.0}\times10^{-3}$		530.1/229	0.72±0.01	0.3	$5.5^{+0.5}_{-0.4}\times10^{-1}$		442.3/229
C4	$2.63^{+0.28}_{-0.24}$	2.0±0.7	$7.4^{+14.0}_{-1.3}\times10^{-5}$		66.9/51	0.74±0.07	< 0.2	$2.6^{+1.2}_{-0.8}\times10^{-2}$		88.7/51
C5	$1.97^{+0.09}_{-0.08}$	3.8±0.3	$2.3\pm0.2\times10^{-4}$		249.4/204	1.34±0.08	1.7±0.2	$1.2^{+0.3}_{-0.2}\times10^{-2}$		322.1/204
C6	2.27±0.14	$5.3^{+0.7}_{-0.6}$	$1.7^{+1.0}_{-0.2}\times10^{-4}$	G	102.9/90	$1.09^{+0.08}_{-0.07}$	2.7±0.4	$1.5^{+0.5}_{-0.4}\times10^{-2}$	G	95.5/90
C7	1.79±0.10	$2.7^{+0.4}_{-0.3}$	$1.4^{+0.7}_{-0.1}\times10^{-4}$	G	139.4/126	$1.40^{+0.11}_{-0.10}$	1.1±0.2	$7.9^{+2.4}_{-1.9}\times10^{-3}$	G	141.3/126
C8	$1.43^{+0.12}_{-0.11}$	$1.5^{+0.4}_{-0.3}$	$6.1^{+7.3}_{-0.7}\times10^{-5}$	G	80.1/82	$1.88^{+0.25}_{-0.20}$	0.5±0.2	$1.7^{+0.8}_{-0.6}\times10^{-3}$	G	79.9/82
C9	$2.71^{+0.24}_{-0.21}$	1.9±0.4	$8.3^{+9.9}_{-1.1}\times10^{-5}$		73.2/54	0.62±0.06	0.3±0.2	$6.0^{+3.0}_{-1.9}\times10^{-2}$		68.2/54
C10	$1.97^{+0.17}_{-0.16}$	$6.8^{+0.9}_{-0.8}$	$1.7^{+1.2}_{-0.3}\times10^{-4}$		81.8/68	$1.38^{+0.17}_{-0.15}$	$4.1^{+0.6}_{-0.5}$	$7.7^{+4.1}_{-2.7}\times10^{-3}$		103.5/68
C11	$2.69^{+0.34}_{-0.31}$	$42.9^{+6.3}_{-5.5}$	$5.2^{+4.9}_{-1.9}\times10^{-4}$	G	46.5/62	$1.37^{+0.18}_{-0.15}$	$29.5^{+3.7}_{-3.3}$	$8.6^{+6.4}_{-3.7}\times10^{-3}$	G	44.3/62
C12	$1.54^{+0.14}_{-0.13}$	0.6±0.3	$3.0^{+7.5}_{-0.3}\times10^{-5}$		85.3/70	$1.40^{+0.15}_{-0.14}$	< 0.1	$2.2^{+0.9}_{-0.6}\times10^{-3}$		100.9/70
C13	$1.81^{+0.10}_{-0.09}$	0.6±0.2	$6.2^{+5.6}_{-0.5}\times10^{-5}$	G	96.5/119	1.08±0.07	< 0.1	$1.0^{+0.3}_{-0.2}\times10^{-2}$	G	140.9/119
C14	$2.28^{+0.13}_{-0.12}$	1.0±0.2	$7.9^{+6.9}_{-0.7}\times10^{-5}$		147.6/108	0.65±0.04	< 0.1	$6.1^{+1.5}_{-1.3}\times10^{-2}$		233.6/108
C15	$1.46^{+0.15}_{-0.14}$	$1.6^{+0.6}_{-0.5}$	$3.7^{+9.6}_{-0.5}\times10^{-5}$	G	54.2/62	$1.77^{+0.28}_{-0.21}$	$0.5^{+0.4}_{-0.3}$	$1.2^{+0.7}_{-0.5}\times10^{-3}$	G	48.2/62
C16	$1.86^{+0.15}_{-0.14}$	4.7±0.9	$1.0^{+1.1}_{-0.2}\times10^{-4}$	G	84.5/78	$1.51^{+0.16}_{-0.14}$	2.1±0.6	$3.8^{+1.7}_{-1.2}\times10^{-3}$	G	85.6/78
C17	$1.38^{+0.15}_{-0.14}$	$0.7^{+0.4}_{-0.3}$	$2.7^{+7.3}_{-0.3}\times10^{-5}$	G	74.2/66	$1.81^{+0.27}_{-0.21}$	< 0.1	$8.9^{+5.4}_{-3.1}\times10^{-4}$		83.5/66
C18	$2.60^{+0.22}_{-0.20}$	2.0±0.4	$5.5^{+9.4}_{-0.7}\times10^{-5}$	G	65.8/74	$0.74^{+0.08}_{-0.07}$	0.1(< 0.3)	$2.0^{+1.1}_{-0.7}\times10^{-2}$	G	74.2/74
C19	$2.60^{+0.17}_{-0.16}$	3.8±0.5	$8.6^{+9.3}_{-1.2}\times10^{-5}$	G	74.5/67	0.87±0.07	1.3±0.3	$1.5^{+0.6}_{-0.4}\times10^{-2}$		65.4/67
C20	$2.35^{+0.17}_{-0.15}$	3.0±0.4	$7.5^{+8.4}_{-0.9}\times10^{-5}$	G	79.3/75	0.93±0.08	$0.9^{+0.3}_{-0.2}$	$1.3^{+0.5}_{-0.4}\times10^{-2}$	G	83.0/75
C21	$2.30^{+0.18}_{-0.17}$	$5.6^{+0.9}_{-0.8}$	$8.4^{+11.4}_{-1.4}\times10^{-5}$		85.6/63	$1.07^{+0.10}_{-0.09}$	$2.8^{+0.6}_{-0.5}$	$8.1^{+3.4}_{-2.4}\times10^{-3}$	G	68.8/63
C22	$5.55^{+0.54}_{-0.45}$	$5.3^{+0.9}_{-0.8}$	$3.2^{+2.2}_{-0.5}\times10^{-4}$		136.9/73	$0.26^{+0.03}_{-0.02}$	1.5±0.5	$6.2^{+6.4}_{-3.0}$		163.0/73

[a]Model names

[b]Photon index for the power-law model

[c]Temperature of the accretion disk at inner radius for the MCD model

[d]Normalization constant for the PL model, in units of photons keV^{-1} cm^{-2} s^{-1} at 1 keV.

[e]Normalization constant for the MCD model, in units of R_{in}(km)^2 cos$\theta/$ D(10 kpc)^2, where R_{in}(km) is the inner radius of the accretion disk in units of km, cosθ is the cosine of the inclination of the accretion disk from the line of sight, and D(10 kpc) is the distance to the source in units of 10 kpc.

[f]Intrinsic absorbing hydrogen column density, in units of 10^{21} cm^{-2}

[g]χ^2 value for the fit and number of degrees of freedom

[h]The "Good" fits, marked with a "G", have $\chi^2_\nu \leq$ 1.2

Table 4.   Statistical tests for single-component fits

Samples (1)	Γ (PL) [a] (2)	K-S (3)	T-test (4)	kT_{in} (MCD) [b] (5)	K-S (6)	T-test (7)	N_H (PL) [c] (8)	K-S (9)	T-test (10)	N_H (MCD) [d] (11)	K-S (12)	T-test (13)
ULX-All vs. Comp-All	2.11±0.89 vs. 2.36±0.92	0.155	0.324	1.44±0.86 vs. 1.14±0.47	0.457	0.126	21.51±0.50 vs. 21.42±0.42	0.74	0.49	21.18±0.66 vs. 21.08±0.55	0.84	0.59
ULX-GF vs. Comp-GF	1.88±0.59 vs. 2.02±0.50	0.731	0.479	1.81±0.99 vs. 1.25±0.37	0.075	0.078	21.56±0.59 vs. 21.44±0.50	0.70	0.55	21.33±0.59 vs. 21.12±0.63	0.32	0.39
ULX-HL vs. ULX-LL	1.70±0.47 vs. 2.44±1.05	**0.011**	**0.005**	1.89±1.02 vs. 1.12±0.50	**0.015**	**0.001**	21.54±0.51 vs. 21.51±0.50	0.75	0.86	21.25±0.70 vs. 21.13±0.64	0.47	0.58
ULX-HL-GF vs. ULX-LL-GF	1.52±0.39 vs. 2.18±0.57	**0.020**	**0.001**	2.26±1.10 vs. 1.22±0.27	**0.022**	**0.012**	21.58±0.60 vs. 21.54±0.61	0.52	0.87	21.52±0.59 vs. 21.09±0.53	0.43	0.11
ULX-HL vs. Comp-All	1.70±0.47 vs. 2.36±0.92	**0.021**	**0.009**	1.89±1.02 vs. 1.14±0.47	**0.050**	**0.003**	21.54±0.51 vs. 21.42±0.42	0.72	0.43	21.25±0.70 vs. 21.08±0.55	0.37	0.45
ULX-HL-GF vs. Comp-GF	1.52±0.39 vs. 2.02±0.50	0.111	**0.009**	2.26±1.10 vs. 1.25±0.37	**0.023**	**0.008**	21.58±0.60 vs. 21.44±0.50	0.48	0.53	21.52±0.59 vs. 21.12±0.63	0.18	0.15
ULX-LL vs. Comp-All	2.44±1.05 vs. 2.36±0.92	0.916	0.699	1.12±0.50 vs. 1.14±0.47	0.896	0.897	21.51±0.50 vs. 21.42±0.42	0.62	0.51	21.13±0.64 vs. 21.08±0.55	0.98	0.81
ULX-LL-GF vs. Comp-GF	2.18±0.50 vs. 2.02±0.50	0.727	0.460	1.22±0.27 vs. 1.25±0.37	0.637	0.843	21.54±0.61 vs. 21.44±0.50	0.93	0.64	21.09±0.53 vs. 21.12±0.63	0.97	0.90

Note. — The table shows statistical comparison using the results from single-component fits. The samples compared in the first column are defined in section 3.1. The abreviations are: GF=Good Fits, with $\chi^2_\nu \leq 1.2$; HL=High Luminosity, ULXs with X-ray (absorbed) luminosity $L_X \geq 5.0\times10^{39}$ erg s^{-1}; LL=Low Luminosity, ULXs with $L_X \leq 5.0\times10^{39}$ erg s^{-1}. For each pair of samples in first column we performed both Kolmogorov-Smirnov (K-S) and the T-test for the means, and we calculate the corresponding probabilities. The significant differences, with probabilities $\leq$ 0.05, are shown in bold. High luminosity ULXs have harder spectra than both low-luminosity ULXs and the comparison sample. There is also marginal evidence that ULXs show higher disk temperatures than the comparison sample if we only consider the good fits in both samples.

[a] Average photon index in the power-law model and one sigma errors

[b] Average inner disk temperature in keV for the MCD model and one sigma errors

[c] Average log Hydrogen column density for the power-law model and one sigma errors in units of cm^{-2}

[d] The same for the MCD model

Table 5.　Two-component spectral fits (model PLMCD)

Source	Γ^a	kT_{in}^b	Norm PL^c	Norm MCD^d	N_H^e	$\Delta\chi^2$/Prob.^{f}	Good fits^g	χ^2/d.o.f.^{h}
(1)	(2)	(3)	(4)	(5)	(6)	(7)	(8)	(9)
ULX sample								
U1	$2.20^{+0.46}_{-0.69}$	$0.28^{+0.17}_{-0.12}$	$4.9^{+13.2}_{-3.2}\times10^{-5}$	$1.1^{+1.0}_{-0.9}$	$5.0^{+2.6}_{-1.4}$	3.1/0.69 (0.69)		65.5/51
U2	$2.52^{+0.26}_{-0.15}$	$1.34^{+0.03}_{-0.06}$	$4.0^{+0.3}_{-0.1}\times10^{-3}$	1.4×10^{-1}	$2.5^{+0.2}_{-0.1}$	397.9/>0.99 (>0.99)		950.9/424
U13	$2.23^{+0.38}_{-0.36}$	$0.13^{+0.04}_{-0.02}$	$3.7^{+10.3}_{-1.3}\times10^{-5}$	$<6.8\times10^3$	$5.0^{+2.0}_{-1.6}$	27.4/>0.99 (>0.99)	G	42.5/48
U18	$1.82^{+0.30}_{-0.17}$	$0.19^{+0.09}_{-0.05}$	$3.0^{+10.2}_{-0.5}\times10^{-5}$	$<4.6\times10^2$	$6.7^{+4.1}_{-2.5}$	8.0/0.94 (0.93)		68.1/51
U19	$1.19^{+0.10}_{-0.14}$	$0.20^{+0.02}_{-0.19}$	$2.1^{+0.2}_{-0.3}\times10^{-5}$	$1.1^{+0.9}_{-1.0}$	<4.4	0.8/0.09 (0.18)		100.0/74
U25	$1.76^{+0.28}_{-0.30}$	$0.19^{+0.08}_{-0.05}$	$1.6^{+1.0}_{-0.5}\times10^{-4}$	$<5.8\times10^2$	$2.0^{+1.4}_{-0.8}$	12.7/>0.99 (>0.99)		87.0/70
U25	$2.16^{+0.19}_{-0.21}$	$0.13^{+0.03}_{-0.02}$	$3.0^{+1.0}_{-0.6}\times10^{-4}$	$<9.8\times10^3$	$3.8^{+1.4}_{-1.0}$	33.7/>0.99 (>0.99)		112.3/93
U33	$2.34^{+0.23}_{-0.37}$	$0.20^{+0.13}_{-0.06}$	$4.0^{+1.4}_{-1.6}\times10^{-4}$	$<4.7\times10^2$	$2.7^{+1.0}_{-0.7}$	3.4/0.73 (0.71)		128.2/102
U34	$3.21^{+0.75}_{-0.72}$	$0.10^{+0.02}_{-0.01}$	$9.6^{+22.2}_{-4.0}\times10^{-5}$	$1.4^{+0.8}_{-0.8}\times10^5$	$9.0^{+0.8}_{-1.1}$	63.6/>0.99 (>0.99)	G	58.0/49
U34	$2.73^{+0.19}_{-0.16}$	0.11 ± 0.01	$2.2^{+0.7}_{-0.3}\times10^{-4}$	$3.1^{+15.0}_{-2.4}\times10^4$	$7.0^{+1.3}_{-1.1}$	149.4/>0.99 (>0.99)		130.1/93
U37	$3.35^{+0.43}_{-0.70}$	$1.14^{+0.15}_{-0.23}$	$1.0^{+2.7}_{-0.3}\times10^{-4}$	$6.1^{+5.9}_{-2.4}\times10^{-3}$	$2.4^{+2.7}_{-1.4}$	11.2/0.98 (0.96)		139.4/104
U39	$1.52^{+0.23}_{-0.29}$	$0.25^{+0.06}_{-0.05}$	$4.8\pm1.6\times10^{-5}$	$3.7^{+8.1}_{-2.4}$	$2.1^{+0.5}_{-0.4}$	54.9/>0.99 (>0.99)	G	142.8/139
U39	$1.28^{+0.23}_{-0.25}$	0.26 ± 0.04	$3.8^{+5.6}_{-1.1}\times10^{-5}$	$3.6^{+5.5}_{-2.0}$	2.1 ± 0.4	83.9/>0.99 (>0.99)	G	148.5/137
U40	$3.77^{+0.50}_{-0.42}$	0.13 ± 0.01	$3.2^{+4.9}_{-0.9}\times10^{-5}$	$4.6^{+3.2}_{-1.4}\times10^2$	$1.8^{+0.3}_{-0.2}$	169.5/>0.99 (>0.99)		146.2/82
U42	1.82	0.13	3.6	5.7	11.6	1.6/0.42 (0.47)		131.4/91
U45	$2.43^{+0.12}_{-0.10}$	0.12 ± 0.01	$3.5^{+0.6}_{-0.4}\times10^{-4}$	$4.2^{+8.9}_{-2.4}\times10^3$	$4.1^{+0.7}_{-0.5}$	225.6/>0.99 (>0.99)	G	212.6/182
U45	$2.28^{+0.18}_{-0.14}$	0.13 ± 0.02	$2.9^{+0.9}_{-0.5}\times10^{-4}$	$2.8^{+13.5}_{-2.0}\times10^3$	$4.7^{+1.2}_{-0.9}$	96.5/>0.99 (>0.99)		160.7/133
Comparison sample								
C1	$3.72^{+0.11}_{-0.08}$	0.10 ± 0.01	$1.2\pm0.1\times10^{-3}$	$1.3^{+3.3}_{-0.9}\times10^5$	8.9 ± 0.4	137.6/>0.99 (>0.99)		239.7/155
C2	$1.73^{+0.13}_{-0.18}$	$0.12^{+0.02}_{-0.01}$	$1.1^{+0.3}_{-0.1}\times10^{-3}$	$1.3^{+12.6}_{-1.1}\times10^4$	$4.7^{+1.6}_{-2.1}$	8.5/0.95 (0.94)		144.4/108
C3	$3.61^{+0.66}_{-0.38}$	$0.82^{+0.03}_{-0.04}$	$1.0^{+0.3}_{-0.1}\times10^{-3}$	$2.1^{+0.5}_{-0.4}\times10^{-1}$	$2.7^{+0.7}_{-0.4}$	189.0/>0.99 (>0.99)		341.1/227
C4	$2.43^{+0.42}_{-0.60}$	$0.18^{+0.17}_{-0.02}$	$6.1^{+14.2}_{-3.5}\times10^{-5}$	$1.7^{+2.9}_{-1.6}\times10^1$	$3.2^{+4.1}_{-2.0}$	3.0/0.68 (0.65)		63.9/49
C5	1.96 ± 0.19	$0.20^{+0.07}_{-0.05}$	$2.3^{+1.3}_{-0.5}\times10^{-4}$	$<7.0\times10^2$	$6.4^{+2.2}_{-1.6}$	12.8/>0.99 (0.98)	G	164.7/139
C9	$2.54(<3.49)$	$0.59^{+0.06}_{-0.14}$	$2.8^{+9.0}_{-2.8}\times10^{-5}$	$5.2^{+11.6}_{-1.2}\times10^{-2}$	$1.1^{+1.4}_{-0.9}$	6.8/0.92 (0.90)		66.4/52
C10	$1.99^{+0.17}_{-0.19}$	$0.18(<0.74)$	$1.8^{+0.4}_{-0.3}\times10^{-4}$	$<8.5\times10^1$	9.7 ± 0.6	2.2/0.59 (0.60)		79.6/66
C12	$1.42^{+0.23}_{-0.51}$	0.31	$2.5^{+7.5}_{-1.5}\times10^{-5}$	$<1.4\times10^{-1}$	$0.6(<1.3)$	1.2/0.39 (0.39)		84.0/68
C14	$1.54^{+0.37}_{-0.52}$	$0.35^{+0.08}_{-0.07}$	$3.0^{+6.9}_{-1.6}\times10^{-5}$	$4.3^{+5.6}_{-2.3}\times10^{-1}$	$0.5^{+0.4}_{-0.3}$	17.4/>0.99 (>0.99)		130.2/106
C22	$3.49^{+0.62}_{-0.56}$	0.12 ± 0.02	$8.9^{+36.8}_{-3.6}\times10^{-5}$	$2.2^{+20.7}_{-1.7}\times10^3$	$5.3^{+1.7}_{-1.1}$	57.4/>0.99 (>0.99)	G	79.6/71

[a]Photon index for the power-law model

[b]Temperature of the accretion disk at inner radius for the MCD model, in keV

[c]Normalization constant for the PL model as in Table 3

[d]Normalization constant for the MCD model, as in Table 3

[e]Intrinsic absorbing Hydrogen column density, in units of 10^{21} cm^{-2}

[f]F-test $\Delta\chi^2$/ confidence levels for the model PLMCD against the PL model alone. The values in parantheses are obtained from simulations, see Section 3.2 for details.

[g]The "good" fits are marked with a "G" as in Table 3

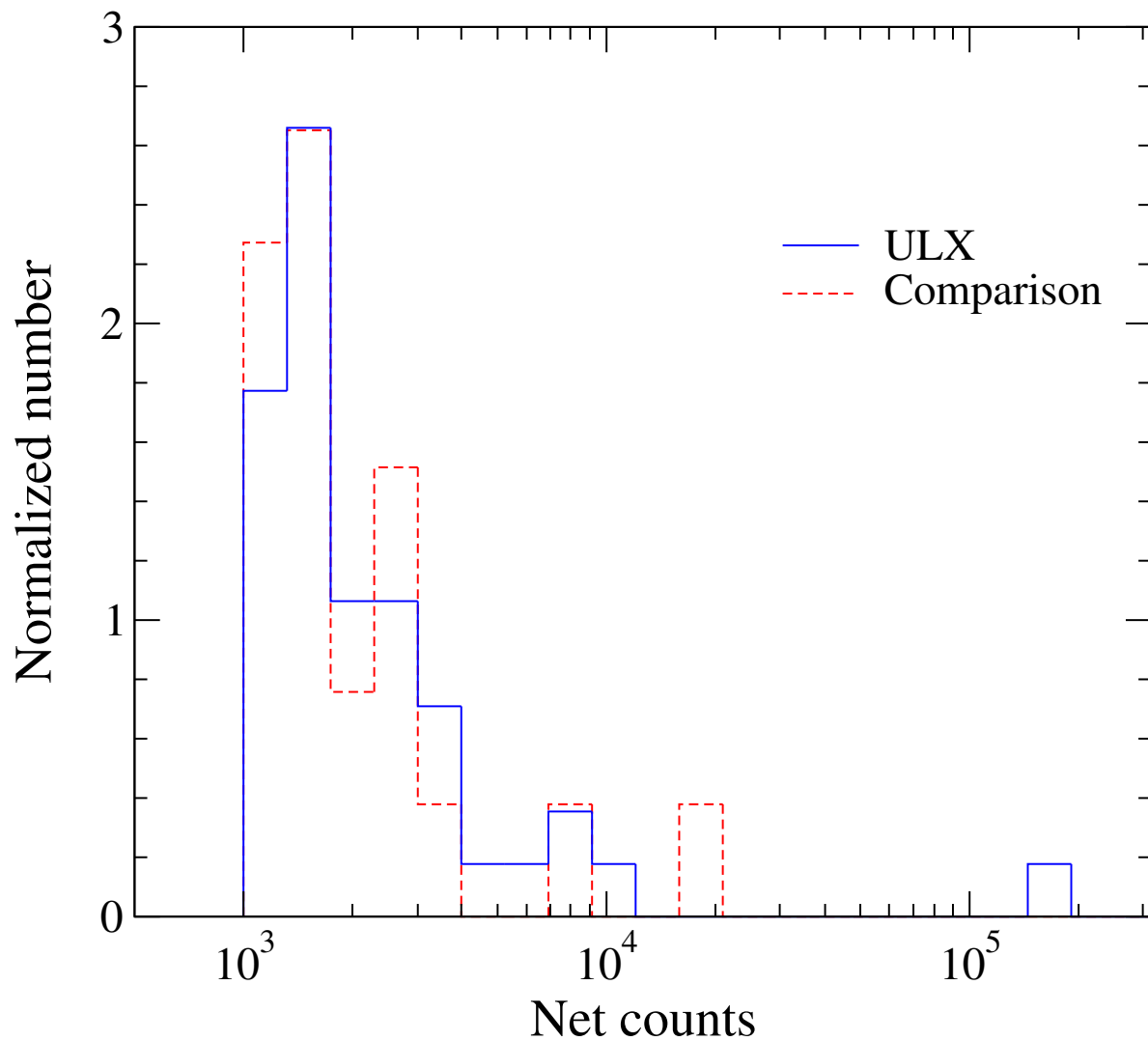[h]χ^2 value for the fit and number of degrees of freedom

Fig. 1.— Normalized histograms of net counts for the ULX and comparison samples. For multiple observations we used the highest number of counts for each object. The histograms are normalized to unit area. The data with counts $>10^5$ is from one source: the long observation of M33 X-8 (U2).
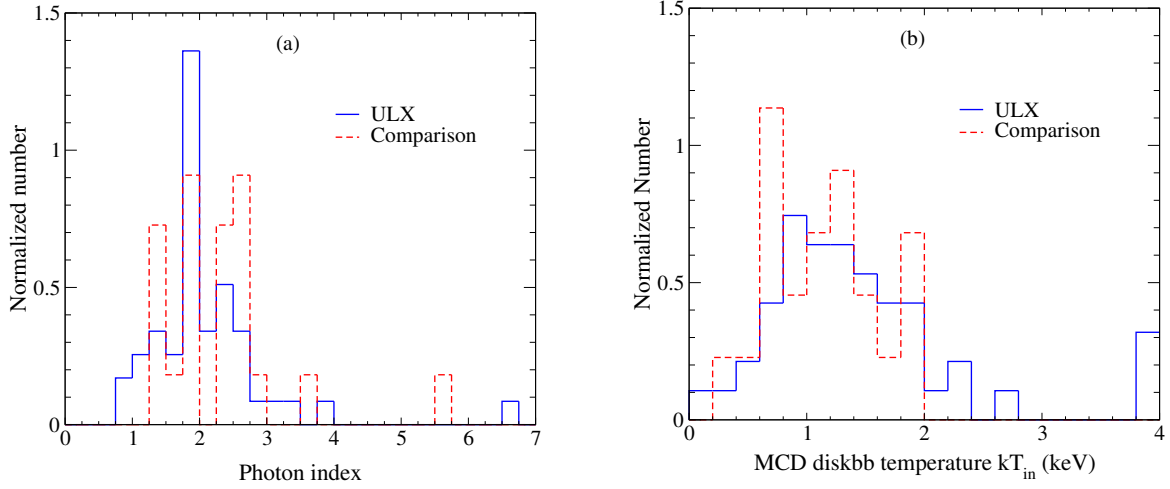
Fig. 2.— Normalized histograms from single-component fits. The histograms are normalized to have a unit area. (a) Photon index distribution from PL fits. (b) Inner disk temperature distribution from MCD fits.
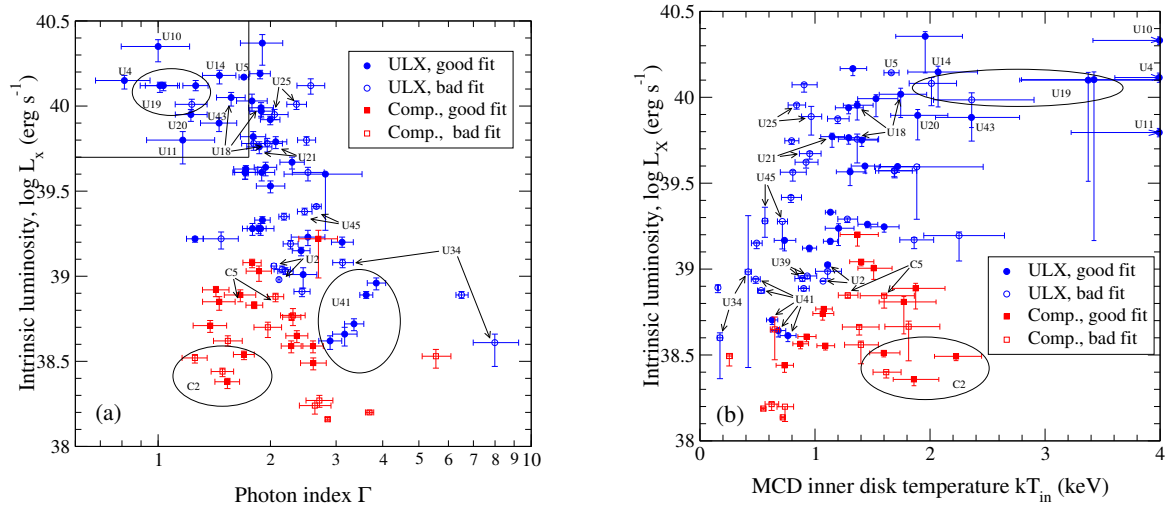

Fig. 3.— (a) Luminosity versus photon index from power-law model fits. (b) Luminosity versus inner disk temperature using the MCD model. In the upper left corner rectangle of the left panel we define a subsample of 9 unique ULXs (U19 has 4 observations). They have luminosities $>5\times10^{39}$ erg s^{-1} and $\Gamma < 1.7$. For clarity, we label only the objects in this ULX subsample plus any objects with multiple observations.
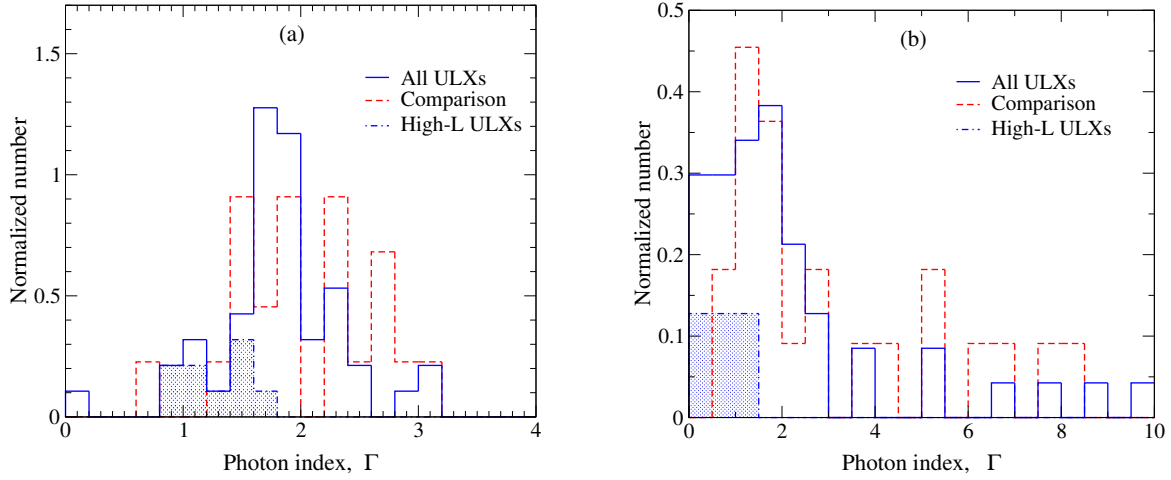
Fig. 4.— Histograms for photon indices from spectral fits with fixed inner disk temperatures, for ULX and lower luminosity samples, both normalized to unit area for easy comparison. We also show the high-luminosity, hard ULXs (filled blue). No significant difference is seen between ULXs and the comparison sample, but the high-luminosity ULXs are distinctly harder (i.e., flatter spectra). a) Model PLMCD0.25 b) Model PLMCD1.0
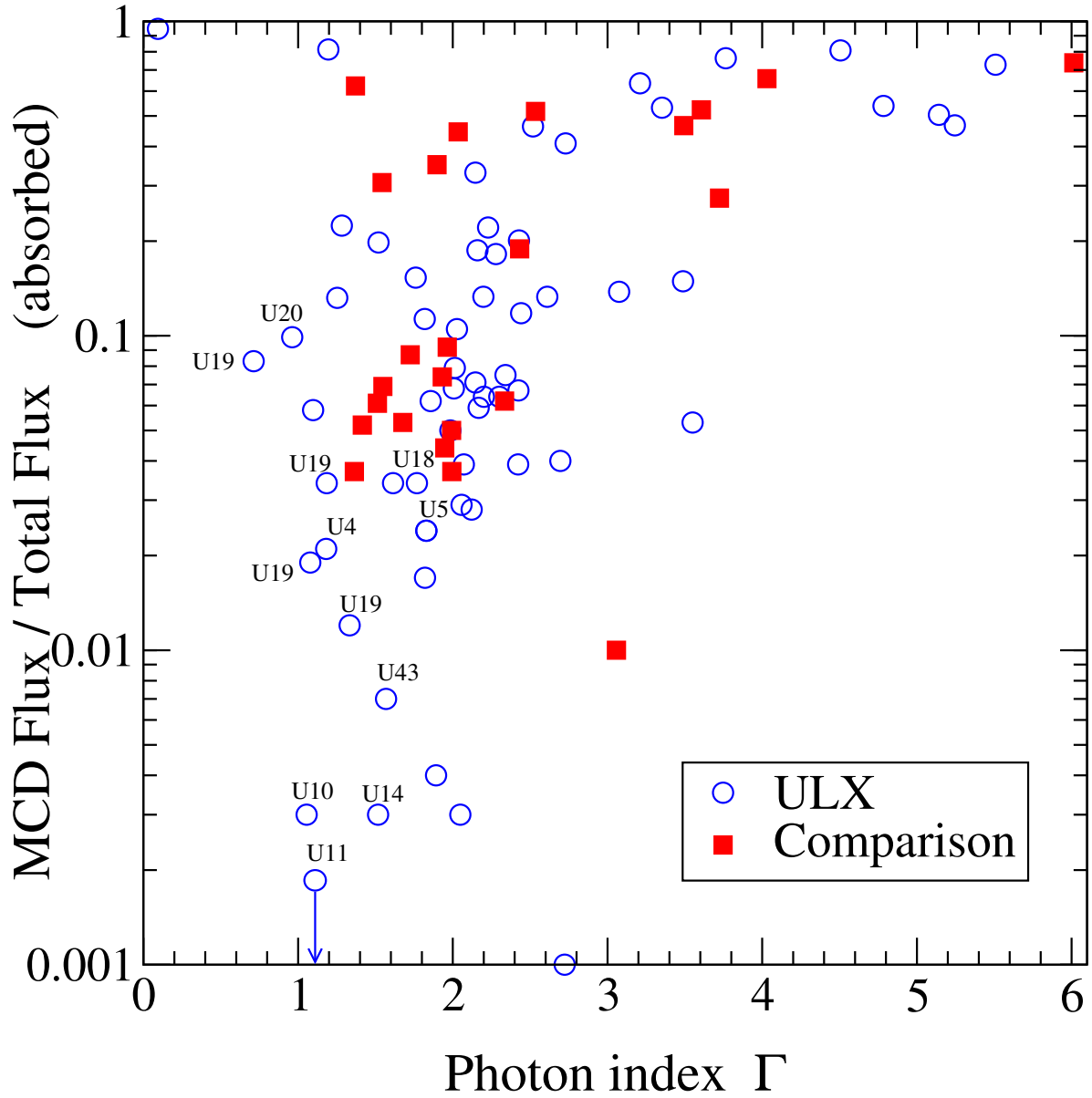
Fig. 5.— The ratio of MCD blackbody flux to the total flux (MCD fraction), plotted against photon index, using the free parameter model PLMCD. The fluxes are absorbed. For clarity, we only label the 9 high-luminosity, hard ULXs as defined in Figure 3a. These have both the hardest spectra and have the lowest flux contribution from the MCD components. For U11 the fraction is below 0.001.
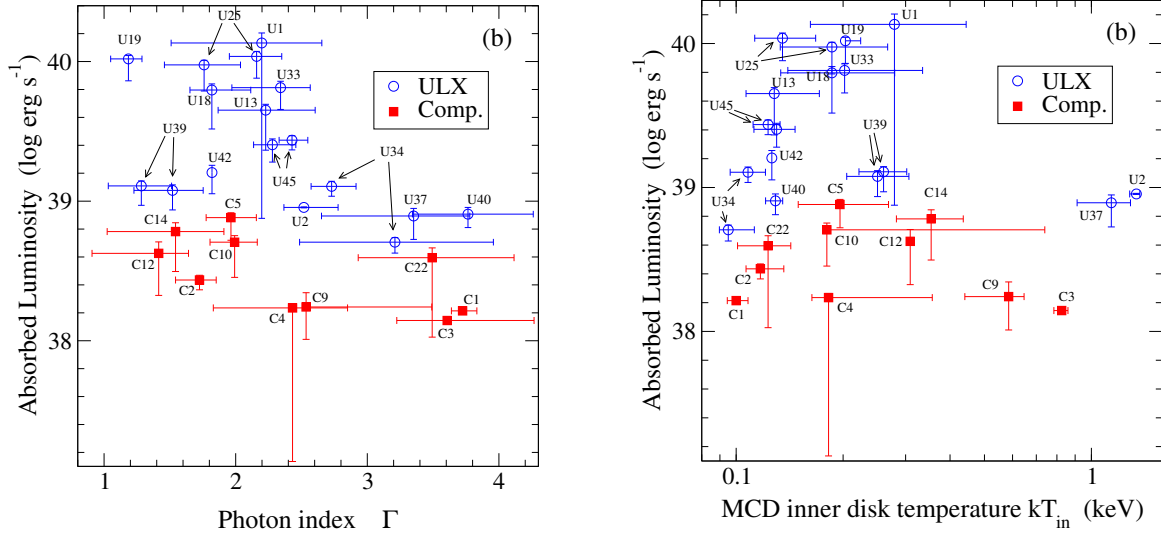
Fig. 6.— Absorbed luminosity scatter plots from the two-component spectral model with free parameters (PLMCD). We present results only for the spectra that did not provide acceptable fits with single component models. a) The photon index dependence. b) Disk temperature dependence.